Kusebauch, C., John, T., Whitehouse, M. J., Klemme, S., Putnis, A. (2015): Distribution of Halogens between Fluid and Apatite during fluid-mediated replacement processes. - *Geochimica et Cosmochimica Acta*, *170*, p. 225-246.

DOI: http://doi.org/10.1016/j.gca.2015.08.023

Distribution of Halogens between Fluid and Apatite during fluid-mediated replacement processes

Christof Kusebauch[1, 5] *, Timm John[2], Martin J. Whitehouse[3], Stephan Klemme[1], Andrew Putnis[1,4]

[1]Institut für Mineralogie, Westfälische Wilhelms-Universität Münster, Corrensstr. 24, D-48149 Münster, Germany

[2]Institut für geologische Wissenschaften, Freie Universität Berlin, Malteser Str. 74-100, 12249 Berlin, Germany

[3]Swedish Museum of Natural History, Box 50007, SE-104 05 Stockholm, Sweden

[4]The Institute for Geoscience Research (TIGeR), Curtin University, Perth, WA 6102 Australia

[5] GeoForschungsZentrum Potsdam, Telegrafenberg, 14473 Potsdam, Germany

*corresponding author: Christof Kusebauch, c.kusebauch@gfz-potsdam.de,

fax +49 251 83 38397

phone +49 251 83 33506

Abstract

Apatite ($Ca_5(PO_4)_3(OH,F,Cl)$) is one of the main host of halogens in magmatic and metamorphic rocks and plays a unique role during fluid-rock interaction as it incorporates halogens (i.e. F, Cl, Br, I) and OH from hydrothermal fluids to form a ternary solid solution of the endmembers F-Apatite, Cl-Apatite and OH-Apatite. Here, we present an experimental study to investigate the processes during interaction of Cl-apatite with different aqueous solutions (KOH, NaCl, NaF of different concentration also doped with NaBr, NaI) at crustal conditions (400-700°C and 0.2 GPa) leading to the formation of new apatite. We use the experimental results to calculate partition coefficients of halogens between apatite and fluid. Due to a coupled dissolution-reprecipitation mechanism new apatite is always formed as a pseudomorphic replacement of Cl-Apatite. Additionally, some experiments produce new apatite also as an epitaxial overgrowth. The composition of new apatite is mainly governed by complex characteristics of the fluid phase from which it is precipitating and depends on composition of the fluid, temperature and fluid to mineral ratio. Furthermore, replaced apatite shows a compositional zonation, which is attributed to a compositional evolution of the coexisting fluid in local equilibrium with the newly formed apatite. Apatite/fluid partition coefficients for F depend on the concentration of F in the fluid and increase from 75 at high concentrations (460 µg/g F) to 300 at low concentrations (46µg/g F) indicating a high compatibility of F in apatite. A correlation of Cl-concentration in apatite with Cl^- concentration of fluid is not observed for experiments with highly saline solutions, composition of new apatite is rather governed by OH^- concentration of the hydrothermal fluid. Low partition coefficients were measured for the larger halogens Br and I and vary between $0.7*10^{-3}$ to $152*10^{-3}$ for Br and $0.3*10^{-3}$-$17*10^{-3}$ for I, respectively. Br seems to have D values of about one order of magnitude higher than I. These data allow an estimation of the D values for the other halogens based on a lattice strain model which displays a sequence with D_F of ~120, D_{OH} of ~100, D_{Cl} of ~2.3 D_{Br} ~0.045, and D_I ~0.0025. Results from this experimental study help to better understand fluid-rock interaction of an evolving fluid, as it enables the composition of hydrothermally derived apatite to be used as a fluid probe for halogens at crustal conditions. It further shows the importance of mineral replacement as one of the key reactions to generate apatite of different composition.

1. INTRODUCTION

Apatite [$Ca_5(PO_4)_3$ (F,OH,Cl)] is one of the most abundant accessory minerals occurring in many different rock types. It is often found to be one of the major hosts of mineral-bound halogens, especially for F, on Earth (Douce et al., 2011; Piccoli and Candela, 2002; Spear and Pyle, 2002; Teiber et al., 2014; Teiber et al., 2015) as well as in extraterrestrial bodies (Boyce et al., 2010; McCubbin et al., 2011; Sarafian et al., 2013). Natural apatite is in most cases a ternary solid solution in which either F, OH or Cl occupy a 6-fold coordinated position between a triangular plane of Ca cations. The incorporation of many different elements (Pan and Fleet, 2002) makes apatite a useful tool for geochemical and isotopic studies, including conventional and fission track dating (Gleadow et al., 2002; Harrison et al., 2002; Li et al., 2012b); deciphering of magma evolution (Boyce and Hervig, 2009; Miles et al., 2014; Webster, 2004) and ore generation. Besides the rare earth elements (REE) (Harlov and Forster, 2002; John et al., 2008; Prowatke and Klemme, 2006) distribution of halogen group elements (mainly F and Cl) between apatite and melt have been the focus of many studies and has been used to calculate halogen concentrations of terrestrial magmas (Marks et al., 2012; Mathez and Webster, 2005; McCubbin et al., 2011; Sarafian et al., 2013; Webster et al., 2009). Furthermore, halogens in apatite allow estimation of water and halogen contents as well as isotopic features of extraterrestrial bodies, e.g. Moon, Mars or meteorites (McCubbin et al., 2010; Sarafian et al., 2013). Although, F and Cl concentrations of apatite are commonly measured and widely used, Br and I data of apatite are extremely scarce (Dong, 2005; Kendrick, 2012; O'Reilly and Griffin, 2000; Teiber et al., 2014; Teiber et al., 2015) but allow to decipher the chemical behavior of halogens in geological processes due to their trace-element character, especially when using spatially resolved analytical techniques.

Halogens influence many geological processes due to their great impact on the petro-physical properties and stabilities of solid and liquid phases (Bartels et al., 2013; Dingwell and Hess, 1998; Douce et al., 2011; Foley et al., 1986; Motoyoshi and Hensen, 2001). They play an important role in the mobilization of otherwise rather immobile trace elements such as high-field-strength elements (HFSE) and REE and are generally regarded as the major player in the formation of ore deposits as the transport and mobility of ore forming elements in hydrothermal fluids are strongly dependent on their complexation by halogens (Williams-Jones et al., 2012). Halogen ratios (i.e. Br/Cl, I/Cl, F/Cl) differ for fluids derived from different geological settings and are used as a fluid tracer to distinguish between different

fluid sources (John et al., 2011; Kendrick et al., 2011). Therefore, a quantification of the amount of all halogens in hydrothermal fluids is needed. Apatite formed in equilibrium with these fluids might provide an easy to use tool for measuring halogen contents of hydrothermal fluids if the distribution of halogens between fluid and apatite is understood.

In addition to the incorporation of halogens into the apatite structure, apatite reacts rather sensitively to changes in the halogen environment in equilibrium with apatite via a coupled dissolution-precipitation process (Jonas et al., 2013; Putnis, 2002; Rendon-Angeles et al., 2000b, c; Yanagisawa et al., 1999). During mineral replacement reactions a parent mineral phase is dissolved into either a thin fluid film or larger fluid filled pore and a more thermodynamically stable mineral phase precipitates from this fluid (Fig. 1) (Pollok et al., 2011; Raufaste et al., 2011). A complex mineral zoning can be formed during replacement as a result of ultra-local equilibrium at the reaction interface (Borg et al., 2014). Natural examples showing a replacement of one phosphate, e.g., Cl-rich apatite or monazite by an apatite of, for instance, OH-rich composition are very common and can be found in almost all rocks undergoing fluid-rock interaction at crustal conditions (Engvik et al., 2009; Harlov et al., 2002; Ondrejka et al., 2012; Upadhyay and Pruseth, 2012).

Herein we present an experimental study performed at 0.2 GPa and temperatures between 400-700°C, to further our understanding of the behavior of halogens during metamorphic replacement reactions. We use the experiments to determine partitioning of F between fluid and apatite at crustal conditions. Furthermore, this paper provides first partitioning data for Br and I, and expands the existing partitioning data for F between apatite and low concentration fluid.

2. EXPERIMENTAL

2.1 Cold-seal pressure vessel (CSPV) Experiments

To obtain replacement reactions we conducted hydrothermal experiments using the cold-seal-pressure-vessel apparatus (CSVP) at the University of Muenster. For all experiments, end member chlor-apatite (Cl-Ap), synthesized following the procedure of Klemme et al. (2013), was used as solid starting material. Synthetic Cl-Ap contains trace amounts of Br (36 µg/g) and I (~1µg/g). For the aqueous solution starting material, various reactive solutions containing NaCl, KOH and NaF were used to investigate the partitioning of different halogens during apatite replacement. Solutions were prepared by dissolving different amounts of chemically pure salts (Alfa Aesar chemicals) in deionized water covering a compositional range of 5-20 wt% NaCl, 100-10000 µg/ml NaF and 0.1-1 M KOH. For some experiments solutions were doped with NaBr and NaI (each 500 or 5000 µg/g in the resulting solution) to examine the partitioning behavior of the large sized halogen ions.

For CSPV experiments, 3-6 grains of inclusion free, colorless, synthetic Cl-Ap crystals are placed together with solution in large volume gold capsules of typically 2 cm length. Capsules are welded shut and left over night in a drying oven at 110°C to check for leakage. Quantities of starting materials were chosen in a way to achieve typical fluid to mineral ratios (F/M) of 50-100 to ensure stable halogen concentrations in the fluid throughout the experiment. Experiments were conducted at different temperatures ranging from 400°C to 700°C, a constant pressure of 0.2 GPa and run duration of either 168 h (exp. without NaBr/NaI) or 336 h and 408 h (exp. with NaBr/NaI). Thermal gradients in CSPVs were less than 5°C for 2 cm long capsules. Experiments were terminated by quenching with cooling rates of ~100°C/min (reaching 100°C after 10 min). A more rapid quench was not necessary as this study focusses on long term fluid mineral interaction. After the experiments the capsules were carefully cut open and solid material was recovered and washed in deionized water. Unfortunately, a recovery of the experimental fluid was not possible due to the low quantity (< 50µl) of fluid. Moreover, a chemical analysis of such a small volume of fluid would be challenging and is practically not feasible.

3. ANALYTICAL METHODS

3.1 Electron probe micro analysis (EPMA)

A JEOL super probe 8900 equipped with 4 wavelength dispersive spectrometers at the University of Muenster was used to examine the chemical composition of the apatite (starting material and run products). Operating conditions for all apatite measurements were 15 kV and 4 nA. Spot sizes varied from 2 to 5 µm and needed to be adjusted for every sample to account for the high porosity in replaced apatite. We are aware of the effect of halogen migration during EPMA measurement caused by the small spot sizes (Goldoff et al., 2012; Stormer et al., 1993). Consequently, a counting time of 10 s for all quantified elements (i.e. F, Ca, Na, K, P and Cl) and a low beam current were chosen to minimize halogen migration due to exposure of the sample to the electron beam. Time-dependent variations of X-ray intensities of F and Cl arising from crystal orientation (Goldoff et al., 2012) were considered by the low counting time. Standardization was done using well established synthetic and natural mineral standards (Ca, P: Durango apatite; F: synthetic Fluoride; Cl: natural Tugtupite; K: natural Sanidin; Na: natural Jadeite). Multiple analyses (n>30) of different apatite standards (including Durango, F-rich and Cl-rich apatite) give analytical uncertainties for each standard of 1% for Ca, 2% for P and 10% for F and Cl (decreases to 5% for high Cl-Apatite), respectively. The relatively high uncertainties for halogens likely reflect halogen migration due to the small spot sizes used also for standard measurements. Furthermore, the unknown exposure history of the standard material to the electron beam can lead to heterogeneities within a single standard.

3.2 Secondary Ion Mass Spectrometry (SIMS)

In addition to the EPMA analyses, halogens (i.e., F, Cl, Br and I) were also quantified using a CAMECA IMS1280 large geometry SIMS instrument at the NORDSIM facility, Swedish Museum of Natural History, Stockholm. Analytical conditions for all measurements closely follow those described by Marks et al. (2012). Briefly, these were a critically focused ~15µm $^{133}Cs^{+}$ primary beam with ~1.8 nA beam current and 20kV impact energy (10kV primary beam, -10 kV secondary beam), low-energy normal-incidence electron flooding to counteract charge build-up on insulating targets, and a mass resolving power (MRP) of 5000 (M/ΔM). Prior to measurement, chosen sites were pre-sputtered for 120s to remove the gold coating

over a 25 by 25µm rastered area and use of a 2500 µm field aperture further minimized surface contamination by restricting the field of view to ca. 22 by 22 µm. Secondary ions were measured either on electron multipliers (< 10^6 cps) or Faraday cups (>10^6 cps) in peak switching mode. Data were acquired over 5 scans with an overall integration time of 120s. At the MRP of 5000, $^{19}F^-$, $^{37}Cl^-$ and $^{127}I^-$ signals were free of molecular interferences; however, neither $^{79}Br^-$ nor $^{81}Br^-$ can be resolved from $CaCl^-$ interferences at MRP < 16000, which cannot be achieved on the IMS1280 without significant transmission loss. Hence, a combined [^{81}Br + $^{44}Ca^{35}Cl$ + $^{46}Ca^{37}Cl$]$^-$ peak was measured and corrected using the intensity of the measured $^{40}Ca^{37}Cl^-$ peak together with the natural isotopic abundances of Ca and Cl. All measured peaks were normalized to the matrix $^{40}Ca^{31}P^-$ signal. Concentrations of halogens were determined relative to Durango apatite using halogen concentrations of 33500µg/g for F (Marks et al., 20012), 4099 µg/g for Cl, 0.84 µg/g for Br and 0.73 µg/g for I. The values for Cl, Br and I were measured by ICP-MS of pyrohydrolyses solution from two Durango apatites (82-91 mg) at the University of Bremen (for a detailed description of the pyrohydrolysis procedure see Barnes et al. (2006) and John et al. (2011) and for ICP-MS measurements see Kusebauch et al. (2015) and John et al. (2011)). Using the method of Bu et al. (2003) for ICP-MS analyses of Br and I, John et al. (2011) showed that halogen concentrations in bulk rock samples can be obtained with this method and values for standard material (i.e., Basalt JB2) can be reproduced.

Chlorine concentration of Durango apatite measured with this method is 4099 ± 363 µg/g, which is in good agreement with reported values ranging between 0.39 and 0.46 wt% (Douce and Roden, 2006; Li et al., 2012a; Marks et al., 2012) determined mainly by EMPA. Additionally, the here reported Cl concentration for Durango apatite give an independent and accurate value that is not affected by complications arising from electron beam exposure of apatite (see section 3.1). Furthermore, it also shows that all Cl was recovered during pyrohydrolysis from Durango apatite indicating also a high recovery yield for the larger and more volatile halogens (i.e., Br and I).

Data of Br and I concentrations for Durango apatite are scarce and range either over orders of magnitude (Br: 0.009-0.06 µg/g, I: 0.001- 0.166 µg/g) (Kendrick, 2012) or are below the detection limit (Br: <0.25 µg/g) of analytical methods used (Ion Chromatography following Pyrohydrolysis) (Marks et al., 2012). Literature values for both elements are lower compared to our values for different reasons: On one hand, it seems that individual Durango apatite

grains are internally homogeneous (this work and Marks et al., 2012) but differ from each other (Boyce and Hodges, 2005; Kendrick, 2012; Marks et al., 2012) which causes analytical problems with the 'noble gas method' (see Kendrick (2012) for further description). On the other hand, the reported detection limit for analytical procedure of Marks et al. (2012) might be underestimated since the quoted amount of material used for pyrohydrolysis (10-25µg) is fairly low. To avoid these complications we increased the amount of material used for pyrohydrolyses (82-91µg) and also conduct ICP-MS measurements, which has a lower detection limit for Br and I in the pyrohydrolysis solution (Br: <0.5ng/ml; I:<0.03 ng/ml correlating to effective detection limits for Durango apatite of 0.6 µg/g for Br and 0.035µg/g for I, respectively) than IC.

Detection limits are estimated based on an average $^{40}Ca^{31}P$ signal of 300,000 cps and a typical ion counter background of 0.05 cps, which is multiplied by three to get the effective detection limit; this yields $6.6*10^{-5}$ µg/g for F, $1.3*10^{-4}$ µg/g for Cl, $3.8*10^{-3}$µg/g for Br and $7.9*10^{-4}$ µg/g for I. Multiple measurements (n=87) of Durango apatite (mineral collection University of Kiel) reveal a standard deviation (1σ) of 7% for F, 5% for Cl, 16% for Br and 4% for I, respectively. The uncertainties are in agreement with published data (Marks et al., 2012) for Durango apatite. However, unreacted synthetic Cl-Ap served as a second possibility to test for reproducibility during measurement. Repeated analyses (n=25) of unreacted Cl-Ap gives a reproducibility (S.D.) of 6% for Cl, 12% for Br and 40% for I, respectively. The high uncertainty for I is likely to be a result of the low concentration in the synthetic Cl apatite, which is at least one order of magnitude lower than the concentration in Durango apatite.

Most SIMS measurements of F and Cl are in good agreement with EPMA measurements within the errors of particular methods. Only Cl measurements of pure Cl-ap with SIMS show higher concentrations compared to EPMA and theoretical calculations of maximum 6.8wt.%. The overestimation might be caused by deviation from an assumed linearity in the two-point concentration working curve, especially considering that Durango apatite used as reference has an order of magnitude lower Cl-concentrations.

4. RESULTS

4.1. Apatite replacement

Replacement of synthetic Cl-Ap by either a solid solution of Cl- and OH- apatite or a solid solution of all three endmembers (Cl-Ap, OH-Ap and F-Ap) was observed in all experiments (Fig. 2 a-f). The extent of replacement depends strongly on composition of the fluid and the fluid / mineral ratio (F/M) in the experiments. In general, a higher concentrated solution (i.e., KOH, NaF and NaCl) and a high F/M ratio leads to a higher extent of replacement. Replacement features can be distinguished into two different groups by the appearance of replaced apatite and the coexisting pores therein. Group A is characterized by a high density of nm- to µm-sized rounded pores, which are sometimes elongated along the crystallographic c axis. The interface between unreacted Cl-Ap and replaced apatite is usually sharp, but can be diffuse in experiments at high temperatures (700°C) with NaCl and NaF solutions. The thickness of the replacement rim around unreacted Cl-Ap is regular and does not depend on the crystallographic orientation (Fig. 2 a, b). Group A replacement is observed in all experiments with NaF solution and also at high temperature runs (>600°C) of NaCl and KOH solutions (Table 1). Group B has larger irregular pores (>5µm), sometimes with a distinct shape representing the prismatic habit of apatite crystals (Fig. 2 c-f). The interface between unaltered Cl-Ap and replaced apatite is irregular in shape, showing fingering and is usually marked by the larger irregular pores (Fig. 2d). Porosity within the replaced apatite seems to be restricted to the large pores as no porosity in the sub-µm range was found with the techniques applied. The outermost rim of replaced grains usually has a higher density of pores compared to inner part of replaced apatite close to the interface. Most KOH experiments and low temperature (<600°C) NaCl experiments show this kind of replacement.

Regardless of group A or group B replacement, porosity-free apatite formed either as an epitaxial overgrowth on replaced apatite (Fig. 2d) or as euhedral crystals from the fluid in some of the experiments. Replacement characteristics of all experiments are summarized in table 1 and dependencies on temperature, fluid/mineral ratio and chemical composition will be discussed in more detail.

4.2. Major element chemistry of replaced apatite measured with EPMA

As the focus of this study is on the halogen behavior during fluid-apatite interaction, halogens and major apatite components (i.e. CaO, P_2O_5) were analyzed. Additionally Na and K were analyzed, as these elements are major components in the solution and can be substituted for Ca in the apatite structure. Molar proportions were calculated on the basis of 12 O for all cations and halogens. The amount of water in apatite (as OH) was calculated assuming ideal mixing of F, Cl and OH on the anion position and a molar proportion of one.

CaO and P_2O_5 concentrations of all apatite analyses vary between 53.9 - 55.3 wt% and 40.6 - 42.4 wt% (2σ), respectively, and apatite typically shows CaO/P_2O_5 of 1.66 (± 0.04). Although individual concentrations of pristine and replaced apatite measurements fall within analytical uncertainties (Ca: 1% and P: 2%), it is interesting to notice that on average, replaced apatite has slightly higher CaO and P_2O_5 concentrations in comparison to the pristine Cl-Ap of 0.7 wt.% and 0.85 wt% difference, respectively (Fig. 3). This might be explained by a Ca and P deficiency (Pan and Fleet, 2002 and references therein) of the starting Cl-Ap synthesized at high temperatures, which is erased by the low temperature replacement reaction.

Na_2O concentrations are typically elevated in replaced apatite from experiments with fluids containing NaCl (up to 0.2 wt% independent of NaCl concentration in solution) and NaF (highly variable up to 2 wt% depending on the NaF concentration of the fluid).

K_2O concentrations of replaced apatite are generally less than 0.06 wt% and independent of KOH concentration of the fluid. Exceptionally high K_2O concentrations of 0.15 to 0.5 wt% were found in apatite that reacted with a combined 0.5 mol KOH and 5000 ppm NaBr/NaI solution and a high F/M ratio (100-128).

4.3. Halogen chemistry of replaced apatite measured with EPMA

All experiments were designed to promote the following replacement reactions:

$$\text{Cl-Ap} + OH^-\,(aq) \rightarrow \text{OH-Ap} + Cl^-\,(aq)$$

$$Ca_5(PO_4)_3\,Cl + OH^-\,(aq) \rightarrow Ca_5(PO_4)_3\,OH + Cl^-\,(aq) \quad (1)$$

and

$$\text{Cl-Ap} + F^-\,(aq) \rightarrow \text{F-Ap} + Cl^-\,(aq)$$

287 $Ca_5(PO_4)_3\,Cl + F^-\,(aq) \rightarrow Ca_5(PO_4)_3\,F + Cl^-\,(aq)$ (2)

288 As there is a complete solid solution between all three end members, i.e. F-, Cl- and OH-
289 apatite, their final composition will be the result of partitioning of the anions between fluid
290 and apatite and the activities of the anions in the whole experimental system.

291 4.3.1. NaCl experiments

292 Interaction of Cl-Ap with a NaCl containing fluid produces an apatite solid solution between
293 Cl-Ap and OH-Ap. To simplify and average the data set, all analysis of run products of each
294 experiment were grouped according to their alteration feature, which is replaced apatite,
295 unreacted Cl-Ap or epitaxial apatite (data summarized in Table 2 and Fig. 4).

296 Experiments conducted at relatively low F/M (fluid/mineral) ratios of ~10 and 1, 600°C and
297 varying NaCl concentration of the solution (0-30%) produced replaced and epitaxial apatite
298 with averaged molar fraction of OH-Ap (X_{OH}=OH/(Cl+OH)) of 0.1 - 0.35 independent of
299 NaCl concentration of the experimental fluid (Fig. 4a). In contrast to the low F/M
300 experiments, an experiment conducted at F/M of 66 and 600°C produced replaced apatite
301 which has a higher average X_{OH} of 0.64 (Fig. 4). A general dependency of apatite composition
302 on temperature is not observed for comparable fluid compositions and F/M (XOH=0.62 ±
303 0.11 at 400°C, 0.27 – 0.35 at 500°C, and ~ 0.5 at 700°C). Individual grains of replaced apatite
304 show a compositional zonation (Fig. 5), which explains the large variability (S.D.) of
305 averaged X_{OH}-values (Fig. 4). In general, detailed transections through individual apatite
306 crystals from center (unreplaced Cl-Ap) to rim (replaced ap) reveal firstly a sharp boundary
307 between unreacted and replaced apatite and secondly increasing X_{OH} values within the
308 replaced apatite towards the rim (Fig. 5a, b, d). In some cases, zonation is not defined by a
309 constant change of composition but by a patchy distribution of different OH-rich and OH-
310 poor segments within replaced apatite with a clear trend of OH-richer segments towards the
311 rim (Fig. 5c). Epitaxial apatite is in general higher in XOH than replaced apatite from the
312 same experiments (Fig. 4). Although, epitaxial apatite is more homogenous in composition
313 (S.D. < 0.1), it can also be zoned. In contrast to replaced apatite, epitaxial apatite has a
314 growth zonation showing a slight decrease in X_{OH} from interface to the former Cl-Ap (earliest
315 epitaxial overgrowth) to the outermost rim (latest overgrowth) (Fig. 5b).

316 4.3.2. KOH experiments

Similar to the NaCl experiments, replacement of Cl-Ap with KOH solution result in the formation of replaced and epitaxial apatite as a solid solution of Cl-Ap and OH-Ap of various proportions depending on composition of fluid, F/M ratio and temperature.

Experiments at different temperatures but similar KOH concentration and F/M ratios show a positive correlation between temperature and the composition of replaced and epitaxial apatite (Fig. 6). When a 0.5 mol KOH solution at a F/M ratio of > 100 was used in the experiments, X_{OH} of replaced apatite increases from intermediate values of ~0.5 at 500°C, to 0.89 at 700°C. The same trends can be observed for 2 other datasets: firstly for the replacement with the same solution (0.5 mol KOH) but a lower F/M ratio of ~50, and secondly with 1 mol KOH solution and F/M ratio between 25 and 52 (Fig. 6). Additionally, increasing amounts of fluid (high F/M) lead to an increase in X_{OH} of the replaced apatite (Fig. 6). Replaced apatite from experiments at F/M of ~100 (0.5 mol KOH) show systematically higher X_{OH}, than replaced apatite from experiments at lower F/M of 50. A systematic trend of apatite composition with KOH concentration of used solutions was not observed.

Although a zonation of replaced apatite is less prominent compared to experiments with NaCl solution, some replaced apatite show a zonation with a higher X_{OH} of the outermost rim, which levels out towards a constant value in the core (Fig. 7).

4.3.3. NaF experiments

Experiments with NaF solution result in the formation of a three end member apatite solid solution as the replacement product (Fig. 8). Epitaxial apatite as observed in NaCl experiments plays a minor role as it is found only in a few experiments as 1-5 µm sized rims. In general, replaced apatite from all NaF experiments is heterogeneous in composition and strongly zoned with highest F concentrations at the outermost rim and decreasing F concentrations towards the core (Fig. 9a, b). The zonation is most prominent in experiments with intermediate NaF concentrations (500-1000 µg/g) and temperatures of 600-700°C where a sharp boundary between synthetic Cl-Ap and replaced apatite is absent (Fig. 9a). For further plotting and data description only measurements from the outermost rim were used as this small rim is thought to be in local equilibrium with the initial experimental bulk solution. The observed porosity evolution and zonation in F composition are indicative for a coupled dissolution-reprecipitation process, in which the replacement reaction starts from the

outermost part (rim) of the pristine mineral by forming a new mineral in local equilibrium with starting solution.

Interaction of synthetic end member Cl-Ap with a low concentration (100 µg/g) NaF solution produces a ternary apatite with intermediate composition for experiments from 500-700°C and an OH-poor apatite at 400°C (Fig. 8). Experiments with intermediate NaF concentrations (500-1000 µg/g) result in the formation of a F-rich apatite with a decreasing Cl and OH component (Fig. 8). Replacement with highly concentrated (1.5-3 wt%) NaF solutions leads to the formation of almost pure F-Ap with a temperature dependent portion of Cl component. At temperatures of 400°C and 500°C X_{Cl} is ~ 0.2, whereas for 600°C and 700°C the run product is almost pure end member F-Ap and only traces of Cl were measured.

4.4. Halogen (Br, I) concentration of apatite measured with SIMS

In addition to EMPA analyses, SIMS analyses were performed to investigate the partitioning of Br and I between newly formed apatite and hydrothermal fluid. For SIMS not all experiments could be measured due to high porosity of replaced apatite from especially NaF experiments. Concentration data can be found in digital appendix A1 and calculated partition values are summarized in Table 1. Starting solutions (KOH: 0.5 mol; NaCl: 5 and 10 wt%; NaF: 0.05 and 1.5 wt %) for the experiments were doped with either 500 or 5000 µg/g NaBr and NaI each. Although, Cl-Ap used as starting material in the experiments was synthesized from chemicals, multiple SIMS measurements of unreacted synthetic Cl-Ap starting material shows a contamination with F, Br and I at a concentration level of 1.1 µg/g (±0.12), 36.4 µg/g (±4.2) and 1.1 µg/g (±0.46), respectively.

4.4.1. NaCl experiments

Replacement with NaCl solution doped with NaBr/NaI results in the formation of replaced apatite with Br and I concentrations ranging from 17-100 µg/g Br and 1-22 µg/g I (Fig. 10a). Epitaxial apatite has lower Br (3-18 µg/g) and I (0.2-1 µg/g) concentrations compared to replaced apatite from the same experiment. Increasing NaBr/NaI concentrations of the experimental solution lead to increasing Br concentration in apatite, but not to increasing I concentrations. Incorporation of Br and I in run products is not temperature dependent as experiments at 500°C and 700°C produce apatite with similar Br and I concentrations.

4.4.2. KOH experiments

Experiments with KOH (0.5mol) as the major solvent and minor amounts of NaBr/NaI (500 and 5000 µg/g) in solution produce replaced apatite ranging from 3-235 µg/g in Br and 0.8-170 µg/g in I (Fig. 10b). In general, Br positively correlates with I within analysis of apatite from the same experiments. Bromine concentrations of epitaxial apatite vary over a relatively large range from 2 µg/g to 82 µg/g, whereas I in this epitaxial apatite is homogenous with concentrations of 0.8-3 µg/g.

4.4.3. NaF experiments

Br and I measurements with SIMS of replaced apatite from 3 different experiments with NaF solution doped with NaBr/NaI reveal concentrations that range from 30-326 µg/g in Br and 0.7- 47 µg/g in I (Fig. 10c). In general, analyzed apatite from individual experiments having a high Br concentration also has a high I concentration.

5. DISCUSSION

5.1. Partitioning of halogens between fluid and apatite

The performed experiments allow the calculation of halogen partition coefficients between a fluid phase and apatite. Partition coefficients D were calculated using following expression:

$$D = \frac{c_{ap}^{halogen}}{c_{fluid}^{halogen}} \quad (3)$$

where $c_{ap}^{halogen}$ is the measured halogen concentration in the apatite and $c_{fluid}^{halogen}$ the concentration of halogens in the coexisting fluid. Due to the limited amount of fluid and quench modifications, $c_{fluid}^{halogen}$ could not be measured during and after replacement reactions and needed to be assumed. The experiments were designed as to justify these assumptions: The high F/M ratios chosen for the experiments lead to almost no changes of incompatible halogens (i.e. Cl, Br and I) as these are mainly stored in the fluid and are not consumed during replacement. Therefore, fluid composition stays virtually constant during fluid-mineral interaction and can be used to calculate partition coefficients. Apatite analyses used for calculations of Cl, Br and I were either from epitaxial apatite or replaced apatite close to the rim as these were most likely in equilibrium with the initial bulk fluid composition. Unlike Cl, Br and I, F is highly compatible and partitions into apatite. Consequently, an F-containing solution will be depleted during interaction with Cl-Apatite. Therefore, partition coefficients for F were calculated using apatite analyses from the outermost zone of replaced apatite, assumed to be, in equilibrium with the starting solution when it was formed.

5.1.1. Fluorine

Based on thermodynamic calculation, Zhu and Sverjensky (1991) found fluorine to be highly compatible in apatite and therefore F-Apatite to be the most abundant apatite end member on Earth. Equilibrium constants for the reaction of OH-Ap to F-Ap derived from these calculations are in agreement with equilibrium constants derived from experimental studies in the buffered system H_2O-portlandite-fluoride-apatite (Zhu and Sverjenskk, 1991 and references therein). Based on this thermodynamic data Piccolo and Candela (1994) calculated concentrations of F in magmatic fluids from coexisting apatite. We would like to stress that their calculated F partitioning between fluid and apatite is based only on theoretical considerations and lacks experimental verification. Experimentally derived partition

coefficients for F between fluid and apatite are hard to quantify as F shifts from a trace element in the fluid to a major component in the apatite and probably does not follow Henry´s law (e.g., Prowatke and Klemme, 2006). Nevertheless, the observed dependence of F concentration in apatite on NaF concentration of the experimental fluid (Fig. 11a) justifies the calculation of an "apparent" partition coefficient for F that is applicable to low concentration fluids. $D_{ap/fluid}$ values calculated from low concentration NaF (100- 1000 µg/g) experiments of this study vary between 50 and 450 independent of temperature but with a clear dependence on F^- concentration of the fluid (Fig. 11b). The dependence on overall F^- concentration is a result of F being a major component in apatite.

To account for the compositional dependence, calculated D values were fitted to an exponential function of the form $D = a * \exp^{(b*x)}$ with a=319 and b= -0.0044, which can be used to predict apparent partition coefficients for different concentration solutions. This fitted function is more of qualitative use as uncertainties become large for very low concentrated experiments at low temperatures (Fig. 11). The temperature dependence of F partitioning proposed by Zhu and Sverjensky (1991) is not confirmed by our experiments and might arise by using a system containing fluorite (CaF_2) as F source in their calculations. The temperature dependent solubility of the fluoride buffer (Tropper and Manning, 2007) imprints in this case the temperature dependence of F partitioning into apatite, which would not be present in a F-unbuffered system.

Compared to F partitioning between apatite and melt (Doherty et al., 2014; Mathez and Webster, 2005; Webster et al., 2009) with reliable $D_{ap/melt}$ values varying from ~2 to < 30 (Fig. 12), the apparent partition coefficient of F between apatite and fluid calculated in this study is one to two orders of magnitude higher. This behavior might be explained by the different bonding/complexing of F in melts and fluids indicating a more compatible behavior of F in melts compared to fluids.

5.1.2. Chlorine

Apatite composition is not dependent on the total Cl^- of the fluid as experiments with different concentration NaCl solutions give the same results within errors (Fig. 4a). The composition of replaced and epitaxial apatite is a function of pH which controls the availability of OH^- in the fluid and, hence, controls the incorporation of OH over Cl into the crystal (see section 5.2.? for discussion). These findings made in the NaCl experiments are in contrast to the theoretical

calculations of Zhu and Sverjensky (1991) that show a dependence of apatite composition on the total Cl^- of the fluid. The high pH sensitivity of Cl incorporation into apatite that is growing from a solution makes it impossible to evaluate meaningful partition coefficients of Cl between complex fluid and apatite. In the more complex system apatite-melt-fluid (Doherty et al., 2014; Mathez and Webster, 2005; Piccoli and Candela, 1994; Webster et al., 2009) partitioning of Cl between all three phases becomes more complicated as it depends not only on the fluid composition but also on the pressure, composition, alkalinity and oxygen fugacity of the melt and exchange properties between all phases. In general, partition coefficients between apatite and melt for Cl range between 0.6 (Mathez and Webster, 2005) and 18 (Doherty et al., 2014) as a function of melt composition (Fig. 12). D values between apatite and magmatic fluid calculated from the same experiments are one to two orders of magnitude lower than between apatite and melt, which might be explained by the different bonding structure of Cl in melt and fluid. In contrast to our experiments, these data were gained in a melt-fluid system in a way that the pH of the fluid is held constant and partitioning of Cl is controlled by the melt properties. This does not apply for hydrothermal and metasomatic systems without a melt which makes it difficult to compare partitioning in the two different settings.

5.1.3. Bromine and Iodine

Br and I partition coefficients were calculated using SIMS measurements of epitaxial apatite as it is free of porosity and grown directly from the fluid. Partition coefficients of Br between NaCl solution and apatite vary between $4.3*10^{-3}$ and $18*10^{-3}$ and seem to depend on Br concentration of the fluid. Calculated D values for I are in the range of $7*10^{-5}$-$2*10^{-3}$. Epitaxial apatite from KOH experiments gives D values in the order of $1.7*10^{-3}$ to $37*10^{-3}$ for Br and $3*10^{-4}$ to $2.6*10^{-3}$ for I, respectively.

Br and I concentrations of replaced apatite scatter over a larger range and are generally higher compared to epitaxial apatite from the same experiment and also higher than in the starting Cl-Ap. Individual measurements of replaced and epitaxial apatite from the same experiment reveal trends showing increasing I with increasing Br concentrations. Hence, the relatively constant I/Br ratios indicate a constant partition coefficient ratio of D_{Br} being more than 10 times higher than D_I (Fig. 10). One possible reason for the large spread of absolute values of Br and I concentrations might be the complex partition behavior of the large halogens during apatite replacement. Differing from epitaxial apatite which is precipitating from the bulk

fluid, replaced apatite precipitates from a more local fluid that might be enriched in Br and I compared to the bulk fluid. Due to the large ion size of Br^- and I^-, transport is not as fast as for the smaller F^-, Cl^- and OH^- ions and heterogeneities in composition between bulk fluid and replacement fluid will not equal out in the same rate. Enrichment of Br^- and I^- in the local replacement fluid results from dissolution of synthetic Cl-Ap containing Br and I into the interfacial fluid, from which only partly new replacement apatite precipitates. Due to the large concentration gradient between bulk fluid and fluid at the replacement interface, all other dissolved components (i.e. Ca^+, PO_4^{3-} and Cl^-) are transported towards the outside of the former Cl-Ap crystal and precipitate there as epitaxial apatite. Br and I stay behind in the local interfacial fluid and become relatively enriched in replaced apatite. Additionally, Br^- and I^- show a strong tendency to bond to surfaces resulting in a low mobility during transport through a highly porous media. The surface affinity might also play a role during replacement when dissolution of Cl-Ap liberates Br and I, which immediately bonds to the surface of reprecipitating apatite. This might also explain the similarity of concentrations between synthetic Cl-Ap and replaced apatite.

Another possibility to explain the elevated Br and I concentrations of replaced apatite compared to epitaxial apatite is the existence of experimental fluid trapped in inclusions that are only present in replaced apatite. Careful cleaning of the sample after cutting and polishing with deionized water and ethanol was applied to remove contaminations from open pores and surface. Nevertheless, closed sub-µm sized pores can be opened during ablation with the Cs-beam of SIMS and release fluid that will be measured together with the apatite. In this case, analyses represent a mixed signal of fluid with a fixed composition (given by the experiment) and replaced apatite with concentrations similar to that of epitaxial apatite. Consequently, compositions of individual points of replaced apatite from each experiment should fall on a mixing line between the two end members, bulk fluid and apatite. This is true for some measurements mainly of replaced apatite from low temperature experiments with KOH and NaCl solution (Fig. 10 a, b), whereas the majority of points are not affected by a contamination with fluid.

Nevertheless, if measurements are affected by contamination with fluid, the lowest values for Br and I represent most likely the composition of replaced apatite. Partition coefficients calculated from replaced apatite are generally higher than for epitaxial apatite and range from $7*10^{-3}$ to $53*10^{-3}$ for Br and $0.3*10^{-3}$ to $17*10^{-3}$ for I in experiments with KOH solution.

514 Experiments with NaCl solution give D values of $13*10^{-3}$- $66*10^{-3}$ for Br and $0.3*10^{-3}$ -
515 $12*10^{-3}$ for I. D values from experiments with NaF solution vary from $13*10^{-3}$ to $192*10^{-3}$ for
516 Br and $1.1*10^{-3}$ to $2.8*10^{-3}$ for I.

517 Recalculated (eq. 3) Nernst partition coefficients of Br between apatite and phosphate melt
518 (Dong, 2005) seem to depend on apatite halogen composition and vary between $20*10^{-3}$ and
519 $70*10^{-3}$ for Cl-apatite and $0.7*10^{-3}$ and $3*10^{-3}$ for F-apatite (Fig. 12). D_{Br} values between
520 apatite and melt agree within the errors with D_{Br} values between apatite and fluid. A
521 correlation of Br incorporation with major components of apatite (i.e., Cl or F) is not observed
522 in our experiments and might result in the first place from the unique compositions used in the
523 phosphate melt experiments.

524 5.1.4. Lattice-strain model

525 The partitioning of elements between mineral phases and melt or fluids can be generally
526 described by the lattice-strain model (Blundy and Wood, 1994, 2003; van Hinsberg et al.,
527 2010), which relates the partition coefficients to ionic radii of elements in the crystallographic
528 positions. The lattice strain model might be also applicable for the anionic halogens, which
529 are either trace elements in solid and fluid but can also be minor or major elements. However,
530 a perfect fit from our results is probably not feasible due to low number of data points and
531 their large uncertainties (i.e. D values of F, Br and I). Nevertheless, we were able to observe a
532 general relationship of D values with effective ionic radii (Fig. 12). For simplification of the
533 lattice-strain model, we assumed F to fit almost perfectly on the crystal site X (i.e., F, Cl, OH)
534 of the apatite structure with the measured D from our experiments. Compared to models
535 derived from phosphate melt/apatite experiments (Dong, 2005), the curve derived from our
536 experiments has a steeper slope, which is to be expected because of the lower temperature for
537 which the curve is constructed. This and the fact that also in apatite-melt-fluid experiments
538 (Doherty et al., 2014; Mathez and Webster, 2005; Webster et al., 2009), D_{Cl} values between
539 apatite and fluid are always lower than D_{Cl} values between apatite and melt (Fig. 12)
540 suggesting that D values of the same ion strongly depend on different binding properties in
541 the fluid (i.e., Na-speciated) compared to melt.

542 Although, the estimation of D values for Cl and OH based on the lattice-strain model is likely
543 more of a qualitative character, it is clear that OH (with an ionic radii of 1.37 Å, similar to F
544 with 1.31 Å) seems to be by far more compatible than Cl (r_i = 1.81 Å). From the presented fit

of the data (Fig. 12), a sequence of D values can be inferred with D_F of ~120, D_{OH} of ~100, D_{Cl} of,~ 2.3, D_{Br} ~ 0.045, and D_I ~0.0025.

5.2. Mechanisms controlling chemical composition of replaced apatite

5.2.1. General replacement

Coupled dissolution-precipitation is a process which occurs during fluid-rock or fluid-mineral interaction and redistributes chemical components and re-equilibrates the fluid/solid system. Various examples have shown that the principal mechanisms of replacement can be extracted from simple salt systems (Pollok et al., 2011; Putnis and Mezger, 2004; Raufaste et al., 2011) but also in more complex systems containing silicates, carbonates, phosphates (Borg et al., 2014; Harlov et al., 2005; Hövelmann et al., 2010; Joachim et al., 2012; Jonas et al., 2014; Milke et al., 2013; Wintsch et al., 2005). Replacement reactions are most effective in fluid-solid systems, in which 1) the system is far from equilibrium and 2) interconnected pore space is created due to volume decrease of newly formed minerals, which enhances the mobility of dissolved species (Putnis and John, 2010).

The pseudomorphic replacement of Cl-Ap by OH-Ap or F-Ap results in the production of porosity within the product phase due to changes in molar volume of the different apatite phases Yanagisawa et al. (1999). Putnis (2002, 2009) proposes an additional mechanism, namely solubility differences between the precursor and replacing phases, to produce porosity. Solubility differences seem to play a role during apatite replacement as observed porosity seems to be significantly greater than the suggested 2.9% due to volume shrinkage. In fact, results from our replacement experiments confirm this additional mechanism to be of importance on a larger scale. It seems as all components of apatite (i.e. Ca, PO_4 groups) are dissolved at the replacement front and transported to the outside of the former crystal, where they precipitate again as epitaxial apatite. The former shape of Cl-Ap is still visible and marked by intersection of porous free epitaxial apatite to highly porous replaced apatite. The occurrence of epitaxial apatite also indicates an efficient interconnectivity of the replacement front with the bulk fluid.

Replacement of apatite can be used to identify changes in coexisting fluid as replaced apatite is thought to be in local equilibrium with the fluid from which it is precipitating. Recently it

has been shown that a complex mineral zoning can be caused by local equilibrium during replacement of calcite by As-bearing OH-Apatite (Borg et al., 2014). Although, the whole fluid-mineral system (i.e., experimental setup) is not in equilibrium, a small subsystem at the reaction interface shows equilibrium conditions during the replacement process. Nevertheless, compositional zonation might become unstable after longer run duration of the experiments and form apatite in equilibrium with the bulk solution. During replacement of Cl-Ap by OH/F-Ap such a homogenization is not observed and the zonation is preserved also after long duration runs. The higher stability of the newly formed apatite compared to the precursor apatite prevents a continuous reaction as long as the chemical-potential gradient between fluid and precursor apatite is higher than that between fluid and replacement apatite. Furthermore, experiments by Rendon-Angeles et al. (2000a) showed that dissolution of F-Ap with highly concentrated KOH solution and precipitation of OH-Ap is kinetically hindered and only occurs above 700°C at reasonable rates. Similarly to the high stability of F-Ap under hydrothermal conditions, OH-Ap is more stable and less soluble than Cl-Ap in most hydrothermal fluids. Consequently, original Cl-Ap replaced by a more stable apatite (OH-Ap or F-Ap) will be kinetically hindered to react again or further with a fluid of only slightly different composition. Therefore replaced apatite records the local equilibrium conditions under which it was formed.

5.2.2 Replacement interface, porosity, and transport

The replacement interface can be generally described as a discrete zone of liquid media in which on one side the parent mineral is dissolved and the daughter mineral precipitates on the opposite side. Raufaste et al. (2011) describe the formation of a complex self-organizing pore structure when KBr is replaced by KCl/KBr solid solution. During reaction of Cl-Ap with NaCl bearing fluid (10 wt%) at 600°C, two different replacement zones at different reaction interfaces can be observed i.e. an outer zone with small pores (type A replacement) and an inner zone with larger pores or cavities (type B). The outline of these cavities are surrounding compartments of replaced apatite in a perfect crystal shape and seem to build a pore structure that is promoting the formation of homogeneous apatite in these compartments. A coupling between morphology and composition of replaced minerals was also observed for fluid inclusions ripened by a coupled dissolution-reprecipitation process in a closed system (Lambrecht and Diamond, 2014). Replaced apatite in these compartments (type B) has lower X_{OH} compared to replaced apatite from the highly porous zone (type A). Furthermore, type B

607 zones with different compartments can be internally zoned with decreasing X_{OH}
608 concentrations of compartments with decreasing distance to the parent Cl-Ap. Similar to
609 KBr/KCl solid solution system where several compartments with different compositions
610 follow one after another, apatite replacement forms different compartments of different
611 composition resulting in a patchy distribution of OH-rich and OH-poor zones, which overall
612 show an increase in X_{OH} towards the rim of the parent Cl-Ap (Fig. 5). The chemical
613 composition of replaced apatite in these compartments strongly depends on the fluid
614 composition in the cavities implying that an internal zonation originates from a changing fluid
615 due to ongoing replacement towards higher Cl^- and/or lower OH^- activities.

616 A chemical zoning is also present in replaced apatite of only type A replacement, generally in
617 experiments with low concentration NaF solution and with NaCl solution at temperatures of
618 700°C. In these examples, zoning follows a change in composition from core to rim and is not
619 related to a patchy distribution of compartments of different composition (Fig. 5d and 9).
620 Chemical zoning in replaced apatite can have two possible causes: 1. diffusion controlled
621 exchange of OH/F and Cl in the fluid between cavity and bulk fluid or solid state diffusion in
622 the replaced apatite or 2. consumption of OH and F from the fluid and simultaneous
623 enrichment of Cl either in the cavity/interfacial fluid only or in the bulk fluid system.

624 5.2.3. Diffusion controlled exchange of OH/F and Cl

625 In KBr/KCl system, a stepwise compositional change of the solid solution is linked to the
626 minimization of strain energies within the newly formed compartments (Raufaste et al.,
627 2011). The limiting rate of the fluid front propagation is controlled by diffusion of Br and Cl
628 in the fluid phase within the porosity connecting the reaction interface with the bulk solution
629 as the replacement thickness L(t) depends on $t^{1/2}$. In the apatite system, the thickness of
630 replacement rims shows no dependence on time and is rather controlled by the amount of
631 fluid in the system (F/M). Furthermore, the calculated rate of replacement and the formation
632 of the zoning are in the range of 10^{-15}-10^{-16} m^2/s, which is several orders of magnitude slower
633 than halogen diffusion in a free fluid at high temperatures. Therefore, it is impossible that the
634 zoning within replaced apatite is produced by diffusion of Cl and OH in the fluid. On the
635 other hand solid state diffusion in apatite is one to two orders of magnitude too slow at
636 temperatures less than 700°C ($<10^{-17}$ m^2/s) even if the crystal orientation (fastest parallel to c)
637 is considered (Brenan, 1993a). Modeling diffusion profiles using extrapolated rates cannot

reproduce the observed compositional profiles in replaced apatite and, therefore, diffusion is not the leading process to produce the observed zonation.

5.2.4. Chemical control and evolving fluid

The second possible explanation of chemical zoning in replaced apatite is the formation of apatite in local equilibrium with a changing fluid composition. As replaced apatite is less soluble than precursor apatite and metastable in a slightly changed fluid, the chemical zonation should record the changing fluid composition during the experimental run. Consequently, only the first formed replacement apatite (outermost rim) will be in equilibrium with a fluid of starting composition. As F and OH are compatible in the apatite structure, they will be enriched in replaced apatite that forms first at the rim and will be thus depleted in the interfacial fluid as well as in the bulk fluid, if the bulk fluid composition is not buffered. Consequently, apatite formed later during replacement will be lower in F and/or OH as it is formed in equilibrium with a fluid that is already depleted. In particular, experiments with low concentration fluids show this evolution and its feedback on the apatite composition. Only in these experiments the consumption of OH and/or F during replacement will lead to a large range of concentrations in the fluid.

NaF solutions

Replacement using NaF solution with concentrations less than 1000 µg/g results in the formation of replaced apatite with a strong zonation (Fig. 9) over the entire rim with thicknesses of 30-100µm.

To further our understanding of how halogens are distributed during replacement processes in our experiments, we use a forward model to calculate the F concentration of a model apatite formed in equilibrium with an evolving fluid. In our model we assume a stepwise replacement of the apatite in small increments going from no replacement to a completely replaced apatite. Replaced apatite is assumed to be nonreactive with the evolving fluid composition and thus does not further react. This assumption is justified by the lower solubility of F-rich apatite compared to the starting Cl-Ap in a still F-containing fluid and the lower chemical-potential gradient between the already replaced apatite and the fluid. During replacement, porosity is formed and stays interconnected to allow fast exchange of ions between the reaction front within the crystal and the bulk fluid.

In the first step of the synthetic model we calculate the chemical composition of a replaced apatite that formed in equilibrium with the starting composition of the fluid in the outermost rim. D values defining the partitioning between fluid and replaced apatite were calculated using measurements from different experiments. The amount of F consumed during the formation of this first replacement rim was subtracted from the total amount of F in the starting fluid. In the next step we used the new fluid composition to calculate the composition of the next apatite rim to be formed, subtracted again the consumed amount of F from the bulk fluid to gain a new fluid composition for the next step. By repeating this process until all parent apatite is replaced, we observe the chemical evolution of the experimental fluid and its feedback on the apatite chemistry. Modeled F concentrations in the replaced apatite decrease as a function of replacement progress. For comparing the modeled results with the compositional zoning observed in the experimental products, we transformed the progress of replacement into rim thicknesses assuming a simplified spherical shape of the apatite and isotropic replacement of this apatite “sphere”. Applying the forward model to specific experiments by taking experimental conditions (i.e. mass of fluid, mass of apatite, concentration of F in starting fluid, crystal size, D values) produces a zonation similar to the observed zonation in replaced apatite (Fig. 13). Differences in length of the zonation profile between model and experiments result from simplifications made in the model such as assuming a spherical shape of crystals or ignoring the anisotropy of replacement observed in natural samples, which does not perfectly match the experiments. Especially, more realistic shapes (instead of an idealised sphere) result in shorter profile length as the sphere shape has the smallest surface to volume ratio. As our model for F consumption is able to explain the observed chemical zonation in replaced apatite, we conclude that the governing process leading to the compositional change in replaced apatite is the chemical evolution of the experimental fluid.

NaCl experiments

In experiments with NaCl, replaced apatite is OH rich/Cl poor in the rims and Cl rich/ OH poor towards the unreacted core (Fig. 5) in either a stepwise or continuous manner. Additionally, epitaxial apatite shows a zonation of the opposite trend (Fig. 5b). As no OH was additionally added, all the OH incorporated into replaced and epitaxial apatite must be generated by dissociation of water molecules. Following the replacement reaction 1 (eq. 1), leads to the consumption of OH from the fluids and the production of HCl. Consequently, the

pH of the fluid will decrease during ongoing replacement and, hence, apatite formed in (local) equilibrium with this evolving fluid will change its chemical composition, even at fluid dominated conditions used in the experiments.

To calculate the evolution of the fluid during ongoing replacement we used two approaches: firstly, we modified our synthetic forward model to predict the pH evolution based on mass balance calculations, and secondly we used the thermodynamic software package PHREEQC (Parkhurst and Appelo, 2013) to model the pH. Unlike F in NaF experiments, where only a limited amount of F is present in the system, OH^- can be permanently produced by dissociation of water molecules. Concentration of OH^- in the NaCl experiments is described by the equilibrium constant of the reaction H_2O reacting to $OH^- + H^+$. The dissociation constant of the starting fluid was calculated for experimental temperatures and pressures using thermodynamic software (i.e. Supcrt92) assuming a neutral solution. Similar to the forward model for F, we used a stepwise approach to model the consumption of OH^- from the fluid due to incorporation into the epitaxial and replaced apatite. After each step, we calculated the pH of the solution from the concentration of H^+ left over from the dissociation of water. Due to the lack of experimental partitioning data for OH^- between fluid and apatite, we were not able to calculate the exact chemical composition of replaced apatite and assumed a replaced apatite with X_{OH} of 1 for each step of replacement. Although a decrease in pH can be predicted from simple mass balance calculations (Fig. 14), the magnitude might be too high (resulting in very low pH values). The main reason for this overestimation is that a mass balance model neglects formation of HCl and different phosphate species in the fluid that will influence the pH. To account for the different species and reactions, we used the PHREEQC software package to model more realistic pH values of the experimental solutions. Although modeling with PHREEQC is limited to temperatures of maximum 250°C, it helps to identify the magnitude of the offset from our mass balance model. Nevertheless, thermodynamic models using increasing temperatures show a general trend towards lower pH. This will result in a closer correspondence between the mass balance model and thermodynamic models.

Figure 14 displays the modeled pH evolution for some experiments with NaCl solution during replacement of Cl-Ap using the experimental conditions as input parameters for the mass balance model (i.e. mass of apatite, mass of fluid, temperature and pressure for calculating the starting pH). For the PHREEQC model the same data were used and only the temperature was changed to 250°C. Both models show that by replacing only the outermost 5 µm of a

simulated, spherical Cl-Apatite crystal the pH of the bulk fluid drops from neutral (~5.5 at 500°C, 0.2 GPa) to acidic. The drop in pH is mainly governed by the individual amounts of fluid and apatite in the experiment and the progress of replacement. From the relatively large changes in OH^- concentration over orders of magnitude in the bulk fluid (displayed by the pH change) we conclude that the process of OH consumption governs the observed zonation in replaced and also in epitaxial apatite. Especially the zonation of epitaxial apatite must display a change in the bulk-fluid composition as this apatite is directly formed from the bulk fluid and therefore under equilibrium conditions that are not controlled by the local environment, e.g., such as an almost isolated pore in newly forming replacement apatite. Accordingly, the zonation of replaced apatite displays the same chemical evolution of the bulk fluid up to a continuous evolution of a trapped and isolated fluid in the larger cavities. Also the stepwise change of the apatite composition can be explained by isolated cavities, which occasionally open and get refreshed with bulk fluid. The composition of replaced apatite is in this case controlled by the local equilibrium in the cavity.

The changing Cl^- fluid concentration during replacement as the reason for the zonation can be neglected as the starting solution is already highly enriched in Cl^- and a complete replacement of all Cl-Ap would change the amount of Cl^- in the solution by only 1-5%, but not over orders of magnitude as is the case for OH^-.

5.3. Temperature dependence of X_{OH}

Despite a dependence on the amount of OH^- in the solution as indicated by the zonation, composition of replaced and epitaxial apatite depends mainly on the experimental temperature (Fig. 4 and 6) and X_{OH} increases with temperature. In general, this behavior is predicted for apatite solid solutions in the system apatite-HCl-H2O from thermodynamics as calculations show an increasing stability of OH-Ap with increasing temperature and pressure at fixed HCl activities (Zhu and Sverjensky, 1991). The assumption of fixed HCl activities applies only in the KOH experiments but not NaCl experiments as in these, HCl is produced during replacement (eq. 1), and, hence, activity of HCl changes strongly throughout the experiment. Therefore, a temperature dependence, although still visible (Fig. 4), is mainly overlain by the constantly changing HCl activity. In contrast, experiments with KOH solution seem to be buffered and HCl activities (and also OH^- activity) are fixed to a certain value, as indicated by the constant composition of replaced apatite. Therefore, the postulated increase of OH-component in apatite with temperature is more prominent and depends on the properties of

764 KOH solution that are changing with increasing temperature. Buffering of activities in the
765 fluid is controlled by the exchange reaction KOH + Cl^- gives KCl + OH^-. Reaction constants
766 for this reaction were calculated for different temperatures using subcrt92 (JOHNSON et al.,
767 1992) and show an increasing stability of KCl and a decreasing stability of KOH leading to
768 the liberation of OH^- with temperature at constant pressures. Assuming a constant
769 partitioning, the resulting increase in OH^- activity with increasing temperature will result in
770 higher X_{OH} of replaced and epitaxial apatite. The absence of a correlation between X_{OH} and
771 KOH concentration of the solution is another indicator for a buffered system.

5.4. Implications

The partitioning behavior of halogens between hydrothermal fluid and apatite has fundamental implications for natural systems containing apatite and for the application and interpretation of partition coefficients. Even in a simple fluid-apatite system, quantitative correlations between fluid chemistry and apatite composition are complex and far from being understood as they are not only a function of concentrations of dissolved species but also of temperature, fluid composition, pH of the fluid and fluid to mineral ratio. The formation of OH-rich apatite from highly concentrated NaCl solutions indicates a lower dependence on total Cl^- than previously thought (Zhu and Sverjensky, 1991) and highlights the importance of the amount of OH^- in the solution, which in turn is a measure of pH of the solution. This observation is in agreement with OH^- being more compatible than Cl^- in the apatite lattice (Fig. 12). Zonation found within the newly formed apatite is a result of pH evolution. A local change of pH also within natural fluids might explain the strong variance in composition of apatite of hydrothermal origin (Engvik et al., 2009; Kusebauch et al., 2015; Roegge et al., 1974). Qualitatively, this means that varying apatite compositions within one sample suite represents evolution of the fluid and apatite reacts relatively sensitively to these changes in the fluid composition. Especially in metasomatic settings, where fluid is pervasively infiltrating the host rock and replenishment is small, the fluid-rock interaction is comparable to batch experiments at low F/M ratios (rock dominated) and evolution of fluid due to ongoing reaction with the host rock will be represented by a zonation of replaced apatite. In contrast, a setting where fluid is highly channelized, will have apatite with a more homogeneous composition as replacement takes place under fluid dominated conditions with a fluid of constant composition. However, on larger length scales a channelized fluid will also change in composition, which enables the use of apatite compositions to investigate the geometry of fluid flow.

Furthermore, interaction of hydrothermal fluids with larger deposits of magmatic Cl-rich apatite would change a hydrothermal fluid to be more acidic and enriched in Cl^-, which in turn affects the solubility and mobility of metals. F^- as a major anion in hydrothermal fluids has a large effect on the solubility of minerals of economic and scientific interest HFSE- and REE-phases (Rapp et al., 2010; Tropper et al., 2013). Additionally, changes in Cl/F ratio of an evolving fluid will lead to differences in element mobility during fluid flow as REE are mobile in Cl rich fluids, whereas HFSE prefer a F-rich fluid. Due to the high partition

804 coefficients, apatite replacement represents an effective process to lower F concentrations
805 over orders of magnitude and, hence, to decrease the dissolution ability of high temperature
806 fluids leading to precipitation of ore forming minerals (Rapp et al., 2010).

807 The importance of the OH-component in apatite and the control of partitioning of OH
808 between fluids or melts and apatite is in general underestimated as most studies focus on the
809 partitioning of F and Cl, omitting OH. Our experiments clearly show that OH partitions into
810 apatite by replacing Cl and that OH has a higher compatibility in the apatite structure at high
811 temperatures regardless of NaCl concentration.

812 Dissociation of water molecules and the resulting pH changes play an important role in apatite
813 –fluid interaction as it delivers OH incorporated into the apatite structure. It might also affect
814 OH incorporation into apatite coexisting with a melt. Even if a concept like pH is not
815 applicable to silicate melts, the amount of dissociation of water molecules in different melts
816 might change locally with composition and oxygen fugacity and will have consequences for
817 the incorporation of OH in apatite crystallizing from this melt. In turn, local changes in
818 halogen and OH activities in melts would produce apatite with varying composition as
819 observed in experiments (Webster et al., 2009) but also in natural apatite (McCubbin et al.,
820 2011), that is only in local equilibrium with a small fraction of melt composition and might
821 not represent the overall bulk composition. Back calculation of melt compositions from
822 apatite composition might be more complicated than previously thought.

823

6. SUMMARY / CONCLUSIONS

Interaction of apatite and fluid via a coupled dissolution-reprecipitation reaction of Cl-Ap produces a ternary apatite solid solution between Cl-Ap, OH-Ap, and F-Ap. The replaced apatite composition is a complex function of the chemical composition of the fluid.

Composition of apatite in NaF containing experiments is controlled by the concentration of F^- in the fluid and partition coefficients between fluid and apatite of F depend on concentration. A temperature dependence of F partioning (as found by other others and predicted by thermodynamic calculations) is not observed. Zonation in F of replaced apatite results from F consumption during ongoing replacement due to the high partition coefficients. Therefore, the zonation in apatite represents the compositional evolution of the fluid phase in the experiment.

In F free systems, the solid solution of OH-Ap and Cl-Ap formed during replacement (and as epitaxial overgrowth) is not governed by the initial fluid composition as neither the total Cl^- in NaCl experiments nor the molarity of OH^- in KOH experiments seem to influence the composition of formed apatite. The observed zonation in replaced and epitaxial apatite in NaCl experiments suggests an evolution in pH of the experimental fluid, whereas the absence of a zonation in KOH experiments indicates a buffering of pH at a constant value.

Br and I are incompatible in the apatite structure and partition coefficients for these halogens are around 0.045 for Br and more than one order of magnitude lower for I. Although, partition values calculated from replaced apatite are in general higher than partition values from epitaxial apatite, they fall within the same range.

In general, the partitioning behavior of halogens between apatite and fluid can be explained by a lattice strain. Partition coefficients derived from this model for different halogens are D_F of ~120, D_{OH} of ~100, D_{Cl} of ~2.3 D_{Br} ~0.045, and D_I ~0.0025 and can be used for calculating compositions of natural hydrothermal fluids. Nevertheless, partitioning of halogens between apatite and fluid is complex and care must be taken when these data is used.

Apatite interacting with aqueous fluid via a coupled dissolution-reprecipitation process provides a powerful tool to trace changes in chemistry of the fluid and therefore can be used to investigate an evolution of fluids in hydrothermal settings.

ACKNOWLEDGEMENTS

We would like to thank the workshops at the Department of Mineralogy at Münster University for support in the laboratories, furthermore Dr. J. Berndt for his help with the EPMA measurements. Kerstin Lindén in Stockholm helped with sample preparation for SIMS. The Nordsim facility is operated as a joint Nordic infrastructure – this is Nordsim contribution ###.

Funding was provided by the German Research Council (DFG) grant [JO 349/3-1].

REFERENCES

Barnes, J.D., Selverstone, J. and Sharp, Z.D. (2006) Chlorine isotope chemistry of serpentinites from Elba, Italy, as an indicator of fluid source and subsequent tectonic history. *Geochem Geophy Geosy* **7**.

Bartels, A., Behrens, H., Holtz, F., Schmidt, B.C., Fechtelkord, M., Knipping, J., Crede, L., Baasner, A. and Pukallus, N. (2013) The effect of fluorine, boron and phosphorus on the viscosity of pegmatite forming melts. *Chem Geol* **346**, 184-198.

Blundy, J. and Wood, B. (1994) Prediction of Crystal-Melt Partition-Coefficients from Elastic-Moduli. *Nature* **372**, 452-454.

Blundy, J. and Wood, B. (2003) Partitioning of trace elements between crystals and melts. *Earth Planet Sc Lett* **210**, 383-397.

Borg, S., Liu, W., Pearce, M., Cleverley, J. and MacRae, C. (2014) Complex mineral zoning patterns caused by ultra-local equilibrium at reaction interfaces. *Geology* **42**, 415-418.

Boyce, J.W. and Hervig, R.L. (2009) Apatite as a monitor of late-stage magmatic processes at Volcan IrazA(o), Costa Rica. *Contrib Mineral Petr* **157**, 135-145.

Boyce, J.W. and Hodges, K.V. (2005) U and Th zoning in Cerro de Mercado (Durango, Mexico) fluorapatite: Insights regarding the impact of recoil redistribution of radiogenic He-4 on (U-Th)/He thermochronology. *Chem Geol* **219**, 261-274.

Boyce, J.W., Liu, Y., Rossman, G.R., Guan, Y.B., Eiler, J.M., Stolper, E.M. and Taylor, L.A. (2010) Lunar apatite with terrestrial volatile abundances. *Nature* **466**, 466-U462.

Brenan, J. (1993a) Kinetics of Fluorine, Chlorine and Hydroxyl Exchange in Fluorapatite. *Chem Geol* **110**, 195-210.

Brenan, J.M. (1993b) Partitioning of Fluorine and Chlorine between Apatite and Aqueous Fluids at High-Pressure and Temperature - Implications for the F and Cl Content of High P-T Fluids. *Earth Planet Sc Lett* **117**, 251-263.

Bu, X.D., Wang, T.B. and Hall, G. (2003) Determination of halogens in organic compounds by high resolution inductively coupled plasma mass spectrometry (HR-ICP-MS). *J Anal Atom Spectrom* **18**, 1443-1451.

Dingwell, D.B. and Hess, K.U. (1998) Melt viscosities in the system Na-Fe-Si-O-F-Cl: Contrasting effects of F and Cl in alkaline melts. *Am Mineral* **83**, 1016-1021.

Doherty, A.L., Webster, J.D., Goldoff, B.A. and Piccoli, P.M. (2014) Partitioning behavior of chlorine and fluorine in felsic melt–fluid(s)–apatite systems at 50 MPa and 850–950 °C. *Chem Geol* **384**, 94-109.

Dong, P. (2005) Halogen-element (F,Cl, and Br) Behaviour in Apatites, Scapolite and sodalite: An experimental Investigation with Field Applications, PhD Thesis. University of Saskatchewan, Saskatoon, pp. 1-222.

Douce, A.E.P. and Roden, M. (2006) Apatite as a probe of halogen and water fugacities in the terrestrial planets. *Geochim Cosmochim Ac* **70**, 3173-3196.

Douce, A.E.P., Roden, M.F., Chaumba, J., Fleisher, C. and Yogodzinski, G. (2011) Compositional variability of terrestrial mantle apatites, thermodynamic modeling of apatite volatile contents, and the halogen and water budgets of planetary mantles. *Chem Geol* **288**, 14-31.

Engvik, A.K., Golla-Schindler, U., Berndt, J., Austrheim, H. and Putnis, A. (2009) Intragranular replacement of chlorapatite by hydroxy-fluor-apatite during metasomatism. *Lithos* **112**, 236-246.

Foley, S.F., Taylor, W.R. and Green, D.H. (1986) The Effect of Fluorine on Phase-Relationships in the System Kalsio4-Mg2sio4-Sio2 at 28 Kbar and the Solution Mechanism of Fluorine in Silicate Melts. *Contrib Mineral Petr* **93**, 46-55.

911 Gleadow, A.J.W., Belton, D.X., Kohn, B.P. and Brown, R.W. (2002) Fission track dating of phosphate
912 minerals and the thermochronology of apatite. *Phosphates: Geochemical, Geobiological, and*
913 *Materials Importance* **48**, 579-630.
914 Goldoff, B., Webster, J.D. and Harlov, D.E. (2012) Characterization of fluor-chlorapatites by electron
915 probe microanalysis with a focus on time-dependent intensity variation of halogens. *Am*
916 *Mineral* **97**, 1103-1115.
917 Harlov, D.E. and Forster, H.J. (2002) High-grade fluid metasomatism on both a local and a regional
918 scale: The Seward Peninsula, Alaska, and the Val Strona di Omegna, Ivrea-Verbano zone,
919 northern italy. part II: Phosphate mineral chemistry. *J Petrol* **43**, 801-824.
920 Harlov, D.E., Forster, H.J. and Nijland, T.G. (2002) Fluid-induced nucleation of (Y+REE)-phosphate
921 minerals within apatite: Nature and experiment. Part I. Chlorapatite. *Am Mineral* **87**, 245-
922 261.
923 Harlov, D.E., Wirth, R. and Forster, H.J. (2005) An experimental study of dissolution-reprecipitation in
924 fluorapatite: fluid infiltration and the formation of monazite. *Contrib Mineral Petr* **150**, 268-
925 286.
926 Harrison, T.M., Catlos, E.J. and Montel, J.M. (2002) U-Th-Pb dating of phosphate minerals.
927 *Phosphates: Geochemical, Geobiological, and Materials Importance* **48**, 523-558.
928 Hövelmann, J., Putnis, A., Geisler, T., Schmidt, B.C. and Golla-Schindler, U. (2010) The replacement of
929 plagioclase feldspars by albite: observations from hydrothermal experiments. *Contrib*
930 *Mineral Petr* **159**, 43-59.
931 Joachim, B., Gardes, E., Velickov, B., Abart, R. and Heinrich, W. (2012) Experimental growth of
932 diopside plus merwinite reaction rims: The effect of water on microstructure development.
933 *Am Mineral* **97**, 220-230.
934 John, T., Klemd, R., Gao, J. and Garbe-Schonberg, C.D. (2008) Trace-element mobilization in slabs due
935 to non steady-state fluid-rock interaction: Constraints from an eclogite-facies transport vein
936 in blueschist (Tianshan, China). *Lithos* **103**, 1-24.
937 John, T., Scambelluri, M., Frische, M., Barnes, J.D. and Bach, W. (2011) Dehydration of subducting
938 serpentinite: Implications for halogen mobility in subduction zones and the deep halogen
939 cycle. *Earth Planet Sc Lett* **308**, 65-76.
940 Johnson, J.W., Oelkers, E.H. and Helgeson, H.C. (1992) Supcrt92 - a Software Package for Calculating
941 the Standard Molal Thermodynamic Properties of Minerals, Gases, Aqueous Species, and
942 Reactions from 1-Bar to 5000-Bar and 0-Degrees-C to 1000-Degrees-C. *Comput Geosci* **18**,
943 899-947.
944 Jonas, L., John, T., King, H.E., Geisler, T. and Putnis, A. (2014) The role of grain boundaries and
945 transient porosity in rocks as fluid pathways for reaction front propagation. *Earth Planet Sc*
946 *Lett* **386**, 64-74.
947 Jonas, L., John, T. and Putnis, A. (2013) Influence of temperature and Cl on the hydrothermal
948 replacement of calcite by apatite and the development of porous microstructures. *Am*
949 *Mineral* **98**, 1516-1525.
950 Kendrick, M.A. (2012) High precision Cl, Br and I determinations in mineral standards using the noble
951 gas method. *Chem Geol* **292**, 116-126.
952 Kendrick, M.A., Phillips, D., Wallace, M. and Miller, J.M. (2011) Halogens and noble gases in
953 sedimentary formation waters and Zn-Pb deposits: A case study from the Lennard Shelf,
954 Australia. *Appl Geochem* **26**, 2089-2100.
955 Klemme, S., John, T., Wessels, M., Kusebauch, C., Berndt, J., Rohrbach, A. and Schmid-Beurmann, P.
956 (2013) Synthesis of trace element bearing single crystals of Chlor-Apatite (Ca-5(PO4)(3)Cl)
957 using the flux growth method. *Chem Cent J* **7**.
958 Kusebauch, C., John, T., Barnes, J., Klügel, A. and Austrheim, H. (2015) Halogen element and stable
959 chlorine isotope fractionation caused by fluid-rock interaction (Bamble sector SE Norway). *J*
960 *Petrol* **in press**.

961 Lambrecht, G. and Diamond, L.W. (2014) Morphological ripening of fluid inclusions and coupled
962 zone-refining in quartz crystals revealed by cathodoluminescence imaging: Implications for
963 CL-petrography, fluid inclusion analysis and trace-element geothermometry. *Geochim*
964 *Cosmochim Ac* **141**, 381-406.
965 Li, C.Y., Zhang, H., Wang, F.Y., Liu, J.Q., Sun, Y.L., Hao, X.L., Li, Y.L. and Sun, W.D. (2012a) The
966 formation of the Dabaoshan porphyry molybdenum deposit induced by slab rollback. *Lithos*
967 **150**, 101-110.
968 Li, Q.L., Li, X.H., Wu, F.Y., Yin, Q.Z., Ye, H.M., Liu, Y., Tang, G.Q. and Zhang, C.L. (2012b) In-situ SIMS U-
969 Pb dating of phanerozoic apatite with low U and high common Pb. *Gondwana Res* **21**, 745-
970 756.
971 Marks, M.A.W., Wenzel, T., Whitehouse, M.J., Loose, M., Zack, T., Barth, M., Worgard, L., Krasz, V.,
972 Eby, G.N., Stosnach, H. and Markl, G. (2012) The volatile inventory (F, Cl, Br, S, C) of
973 magmatic apatite: An integrated analytical approach. *Chem Geol* **291**, 241-255.
974 Mathez, E.A. and Webster, J.D. (2005) Partitioning behavior of chlorine and fluorine in the system
975 apatite-silicate melt-fluid. *Geochim Cosmochim Ac* **69**, 1275-1286.
976 McCubbin, F.M., Jolliff, B.L., Nekvasil, H., Carpenter, P.K., Zeigler, R.A., Steele, A., Elardo, S.M. and
977 Lindsley, D.H. (2011) Fluorine and chlorine abundances in lunar apatite: Implications for
978 heterogeneous distributions of magmatic volatiles in the lunar interior. *Geochim Cosmochim*
979 *Ac* **75**, 5073-5093.
980 McCubbin, F.M., Steele, A., Hauri, E.H., Nekvasil, H., Yamashita, S. and Hemley, R.J. (2010) Nominally
981 hydrous magmatism on the Moon. *P Natl Acad Sci USA* **107**, 11223-11228.
982 Miles, A.J., Graham, C.M., Hawkesworth, C.J., Gillespie, M.R., Hinton, R.W. and Bromiley, G.D. (2014)
983 Apatite: A new redox proxy for silicic magmas? *Geochim Cosmochim Ac* **132**, 101-119.
984 Milke, R., Neusser, G., Kolzer, K. and Wunder, B. (2013) Very little water is necessary to make a dry
985 solid silicate system wet. *Geology* **41**, 247-250.
986 Motoyoshi, Y. and Hensen, B.J. (2001) F-rich phlogopite stability in ultra-high-temperature
987 metapelites from the Napier Complex, East Antarctica. *Am Mineral* **86**, 1404-1413.
988 O'Reilly, S.Y. and Griffin, W.L. (2000) Apatite in the mantle: implications for metasomatic processes
989 and high heat production in Phanerozoic mantle. *Lithos* **53**, 217-232.
990 Ondrejka, M., Uher, P., Putis, M., Broska, I., Bacik, P., Konecny, P. and Schmiedt, I. (2012) Two-stage
991 breakdown of monazite by post-magmatic and metamorphic fluids: An example from the
992 Veporic orthogneiss, Western Carpathians, Slovakia. *Lithos* **142**, 245-255.
993 Pan, Y.M. and Fleet, M.E. (2002) Compositions of the apatite-group minerals: Substitution
994 mechanisms and controlling factors. *Phosphates: Geochemical, Geobiological, and Materials*
995 *Importance* **48**, 13-49.
996 Parkhurst, D.L. and Appelo, C.A.J. (2013) Description of input and examples for PHREEQC version 3--A
997 computer program for speciation, batch- reaction, one-dimensional transport, and inverse
998 geochemical calculations. U.S. Geological Survey Techniques and Methods, book 6, chap. A43
999
1000 Piccoli, P. and Candela, P. (1994) Apatite in Felsic Rocks - a Model for the Estimation of Initial Halogen
1001 Concentrations in the Bishop Tuff (Long Valley) and Tuolumne Intrusive Suite (Sierra-Nevada
1002 Batholith) Magmas. *Am J Sci* **294**, 92-135.
1003 Piccoli, P.M. and Candela, P.A. (2002) Apatite in igneous systems. *Phosphates: Geochemical,*
1004 *Geobiological, and Materials Importance* **48**, 255-292.
1005 Pollok, K., Putnis, C.V. and Putnis, A. (2011) Mineral Replacement Reactions in Solid Solution-
1006 Aqueous Solution Systems: Volume Changes, Reactions Paths and End-Points Using the
1007 Example of Model Salt Systems. *Am J Sci* **311**, 211-236.
1008 Prowatke, S. and Klemme, S. (2006) Trace element partitioning between apatite and silicate melts.
1009 *Geochim Cosmochim Ac* **70**, 4513-4527.
1010 Putnis, A. (2002) Mineral replacement reactions: from macroscopic observations to microscopic
1011 mechanisms. *Mineral Mag* **66**, 689-708.

Putnis, A. (2009) Mineral Replacement Reactions. *Thermodynamics and Kinetics of Water-Rock Interaction* **70**, 87-124.
Putnis, A. and John, T. (2010) Replacement Processes in the Earth's Crust. *Elements* **6**, 159-164.
Putnis, C.V. and Mezger, K. (2004) A mechanism of mineral replacement: Isotope tracing in the model system KCl-KBr-H2O. *Geochim Cosmochim Ac* **68**, 2839-2848.
Rapp, J.F., Klemme, S., Butler, I.B. and Harley, S.L. (2010) Extremely high solubility of rutile in chloride and fluoride-bearing metamorphic fluids: An experimental investigation. *Geology* **38**, 323-326.
Raufaste, C., Jamtveit, B., John, T., Meakin, P. and Dysthe, D.K. (2011) The mechanism of porosity formation during solvent-mediated phase transformations. *P Roy Soc a-Math Phy* **467**, 1408-1426.
Rendon-Angeles, J.C., Yanagisawa, K., Ishizawa, N. and Oishi, S. (2000a) Conversion of calcium fluorapatite into calcium hydroxyapatite under alkaline hydrothermal conditions. *J Solid State Chem* **151**, 65-72.
Rendon-Angeles, J.C., Yanagisawa, K., Ishizawa, N. and Oishi, S. (2000b) Effect of metal ions of chlorapatites on the topotaxial replacement by hydroxyapatite under hydrothermal conditions. *J Solid State Chem* **154**, 569-578.
Rendon-Angeles, J.C., Yanagisawa, K., Ishizawa, N. and Oishi, S. (2000c) Topotaxial conversion of chlorapatite and hydroxyapatite to fluorapatite by hydrothermal ion exchange. *Chem Mater* **12**, 2143-2150.
Roegge, J.S., Logsdon, M.J., Young, H.S., Barr, H.B., Borcsik, M. and Holland, H.D. (1974) Halogens in Apatites from Providencia Area, Mexico. *Econ Geol* **69**, 229-240.
Sarafian, A.R., Roden, M.F. and Patino-Douce, A.E. (2013) The volatile content of Vesta: Clues from apatite in eucrites. *Meteorit Planet Sci* **48**, 2135-2154.
Shannon, R.D. (1976) Revised Effective Ionic-Radii and Systematic Studies of Interatomic Distances in Halides and Chalcogenides. *Acta Crystallogr A* **32**, 751-767.
Spear, F.S. and Pyle, J.M. (2002) Apatite, monazite, and xenotime in metamorphic rocks. *Phosphates: Geochemical, Geobiological, and Materials Importance* **48**, 293-335.
Stormer, J.C., Pierson, M.L. and Tacker, R.C. (1993) Variation of F-X-Ray and Cl-X-Ray Intensity Due to Anisotropic Diffusion in Apatite during Electron-Microprobe Analysis. *Am Mineral* **78**, 641-648.
Teiber, H., Marks, M.A.W., Wenzel, T., Siebel, W., Altherr, R. and Markl, G. (2014) The distribution of halogens (F, Cl, Br) in granitoid rocks. *Chem Geol* **374–375**, 92-109.
Teiber, H., Scharrer, M., Marks, M.A.W., Arzamastsev, A.A., Wenzel, T. and Markl, G. (2015) Equilibrium partitioning and subsequent re-distribution of halogens among apatite–biotite–amphibole assemblages from mantle-derived plutonic rocks: Complexities revealed. *Lithos* **220–223**, 221-237.
Tropper, P. and Manning, C.E. (2007) The solubility of fluorite in H2O and H2O-NaCl at high pressure and temperature. *Chem Geol* **242**, 299-306.
Tropper, P., Manning, C.E. and Harlov, D.E. (2013) Experimental determination of CePO4 and YPO4 solubilities in H2O-NaF at 800 degrees C and 1 GPa: implications for rare earth element transport in high-grade metamorphic fluids. *Geofluids* **13**, 372-380.
Upadhyay, D. and Pruseth, K.L. (2012) Fluid-induced dissolution breakdown of monazite from Tso Morari complex, NW Himalayas: evidence for immobility of trace elements. *Contrib Mineral Petr* **164**, 303-316.
van Hinsberg, V.J., Migdisov, A.A. and Williams-Jones, A.E. (2010) Reading the mineral record of fluid composition from element partitioning. *Geology* **38**, 847-850.
Webster, J.D. (2004) The exsolution of magmatic hydrosaline chloride liquids. *Chem Geol* **210**, 33-48.
Webster, J.D., Tappen, C.M. and Mandeville, C.W. (2009) Partitioning behavior of chlorine and fluorine in the system apatite-melt-fluid. II: Felsic silicate systems at 200 MPa. *Geochim Cosmochim Ac* **73**, 559-581.

1063 Williams-Jones, A.E., Migdisov, A.A. and Samson, I.M. (2012) Hydrothermal Mobilisation of the Rare
1064 Earth Elements - a Tale of "Ceria" and "Yttria". *Elements* **8**, 355-360.
1065 Wintsch, R.P., Aleinikoff, J.N. and Keewook, Y. (2005) Foliation development and reaction softening
1066 by dissolution and precipitation in the transformation of granodiorite to orthogneiss,
1067 Glastonbury Complex, Connecticut, USA. *Can Mineral* **43**, 327-347.
1068 Yanagisawa, K., Rendon-Angeles, J.C., Ishizawa, N. and Oishi, S. (1999) Topotaxial replacement of
1069 chlorapatite by hydroxyapatite during hydrothermal ion exchange. *Am Mineral* **84**, 1861-
1070 1869.
1071 Zhu, C. and Sverjensky, D.A. (1991) Partitioning of F-Cl-Oh between Minerals and Hydrothermal
1072 Fluids. *Geochim Cosmochim Ac* **55**, 1837-1858.

1073

1074

1075 Figures:

1076 Fig. 1. General schematic illustration of apatite replacement at different times during
1077 experiment

1078

1079 Fig. 2. Back-scatter electron (BSE) images of replaced and epitaxial apatite after experiments;
1080 a) type A replacement with NaF solution at 600°C showing µm sized pores and sharp
1081 interface between pristine and replaced apatite (Exp. 67). b) type A replacement with NaF
1082 solution at 700°C with a diffuse interface (Exp. 58). c) type B replacement with NaCl solution
1083 at 500°C showing segments of replaced apatite and large pores (Exp. 74). d) detailed image of
1084 epitaxial and replaced apatite as in c) showing segments of replaced apatite surrounded by
1085 pores tracing the prismatic shape of apatite (Exp. 63). e) type B replacement with KOH
1086 solution at 500°C (Exp. 59). f) detailed image of replaced apatite as in e) with pores tracing
1087 the shape of apatite (Exp. 59).

1088

1089 Fig. 3. Distribution of CaO and P_2O_5 concentrations of synthetic unreacted Cl-Ap (blue +) and
1090 newly formed (epitaxial and replaced) apatite (red dots) with histograms of EPMA
1091 measurements of each group

1092

1093 Fig. 4. Composition of replaced and epitaxial apatite from experiments with different
1094 concentrated NaCl solutions as function of a) fluid composition of experiments at 600°C and
1095 different fluid-mineral ratios; partitioning data from other experimental studies (Brenan,
1096 1993b; Mathez and Webster, 2005; Webster et al., 2009) showing a different behavior of
1097 apatite composition with NaCl concentration of fluid phase. b) Temperature of experiments
1098 with 10 wt% NaCl solution and different fluid-mineral ratios. Errors are 1σ of EMPA
1099 measurements of replaced or epitaxial apatite for each experiment.

1100

1101 Fig. 5. Compositional zoning of replaced and epitaxial apatite from NaCl experiments. a)
1102 compositional line scan (X_{OH}) of run products replaced at 600°C and 10wt% NaCl sol. of type
1103 A (Exp. 88). b) at 500°C and 5wt% NaCl sol. of type B (Exp. 63). c) Cl-map of replaced and

epitaxial apatite from the same experiment as in b) and Fig. 2d) showing segments of replaced apatite with a different composition. d) Compositional line scan of apatite replaced at 700°C and 10wt% NaCl sol. of type A (Exp. 76).

Fig. 6. Composition (XOH) of replaced and epitaxial apatite from experiments with KOH solution

Fig. 7. Compositional line scan of apatite replaced with 0.5 mol KOH at 500°C from unreacted core to rim showing a homogenous composition of replaced apatite (Exp. 59).

Fig. 8. Ternary composition of replaced apatite from experiments with different concentrated NaF solutions at varying temperatures.

Fig. 9. Compositional profile (X_F) of replaced apatite from NaF experiments at a) 700°C and 500µg/g NaF showing no clear interface between pristine and replaced apatite (Exp. 58) and b) 600°C and 500 µg/g NaF showing a clear interface (Exp. 67).

Fig. 10. Br and I concentrations of replaced and epitaxial apatite from experiments with different solutions a) NaCl; b) KOH; c) NaF. Straight lines display I/Br ratios of either 1, 10 or 50 and apatite measurements following these lines indicate a constant partitioning of Br and I between fluid and new apatite; blue lines display mixing lines between a replaced or epitaxial apatite and experimental fluid, apatite measurements following this line are likely contaminated with Br and I from fluid filled inclusions.

Fig. 11. a) Fluorine concentration of replaced apatite from experiments with NaF solutions. b) distribution coefficients between NaF containing fluid and apatite as a function of fluid composition.

Fig. 12. Onuma plot of experimentally derived partition coefficients for halogens in apatite-melt and apatite-fluid systems (with 1σ); effective ionic radii taken from Shannon (1976); dashed green lines: lattice-strain model of Dong (2005) based on molar D values; solid black line: fit of lattice-strain model for our data assuming F to fit ideal on the crystal site.

Fig. 13. F consumption model adapted to experimental conditions of a) exp 58 with 500µg/g NaF, F/M ratio 34, 70µm particle size (also see Fig. 9a) and b) exp 67 with 500µg/g NaF, F/M ratio 50, particle size 200µm. Distribution coefficients are either fixed or calculated for changing fluid composition. Observed compositional zonation of replaced apatite can be reproduced by F consumption from fluid.

Fig. 14. Modeled pH evolution of a fluid during replacement of Cl-Ap by OH-rich apatite assuming that a) OH^+ from deionization of water is consumed and HCl is formed (mass balance model) and b) from thermodynamic modeling using PHREEQC at 250°C; pH is decreasing with increasing progress of replacement and depends only on F/M ratio.

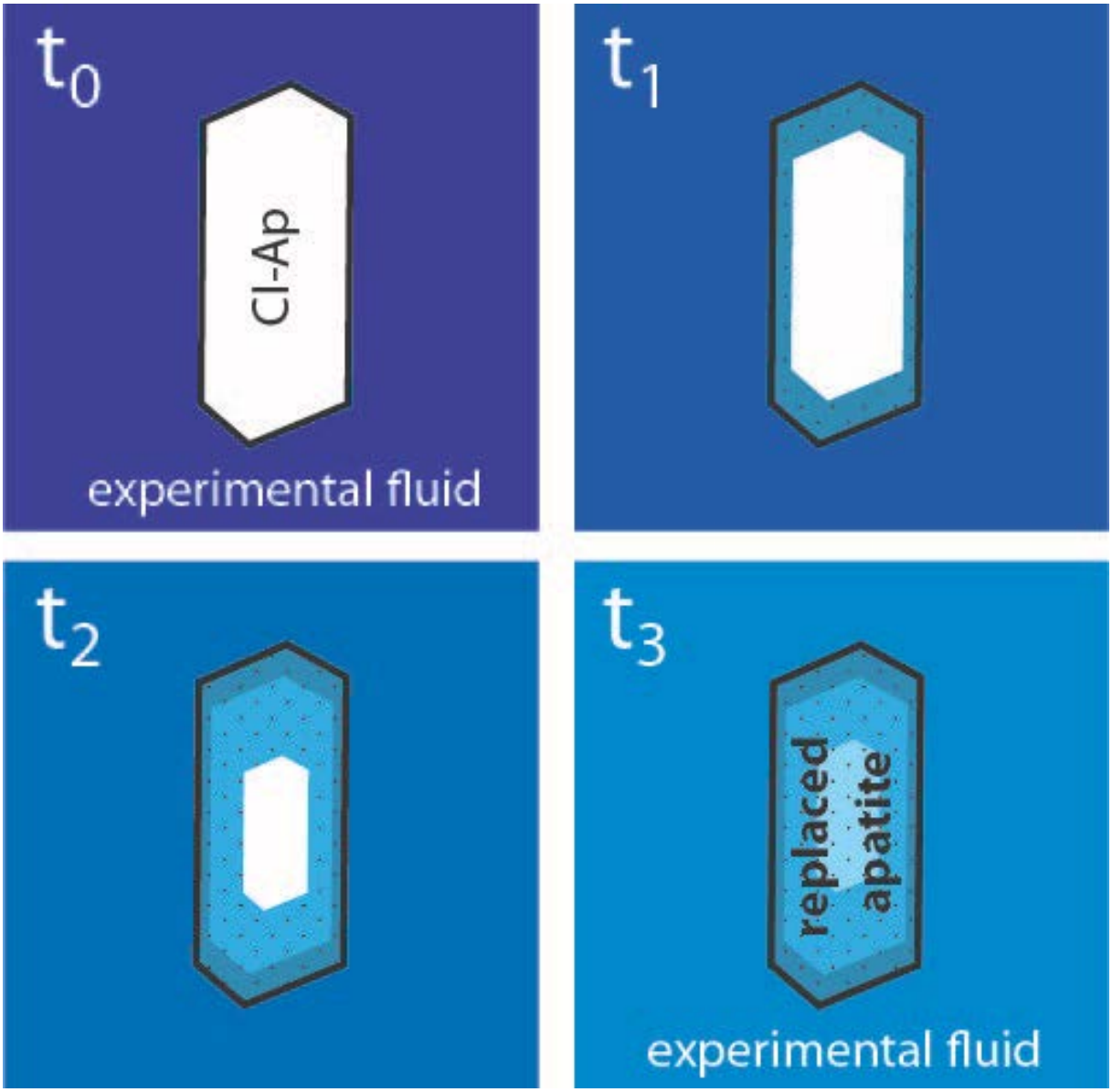
t0
Cl-Ap
experimental fluid
t1
t2
t3
replaced apatite
experimental fluid

Figure 1

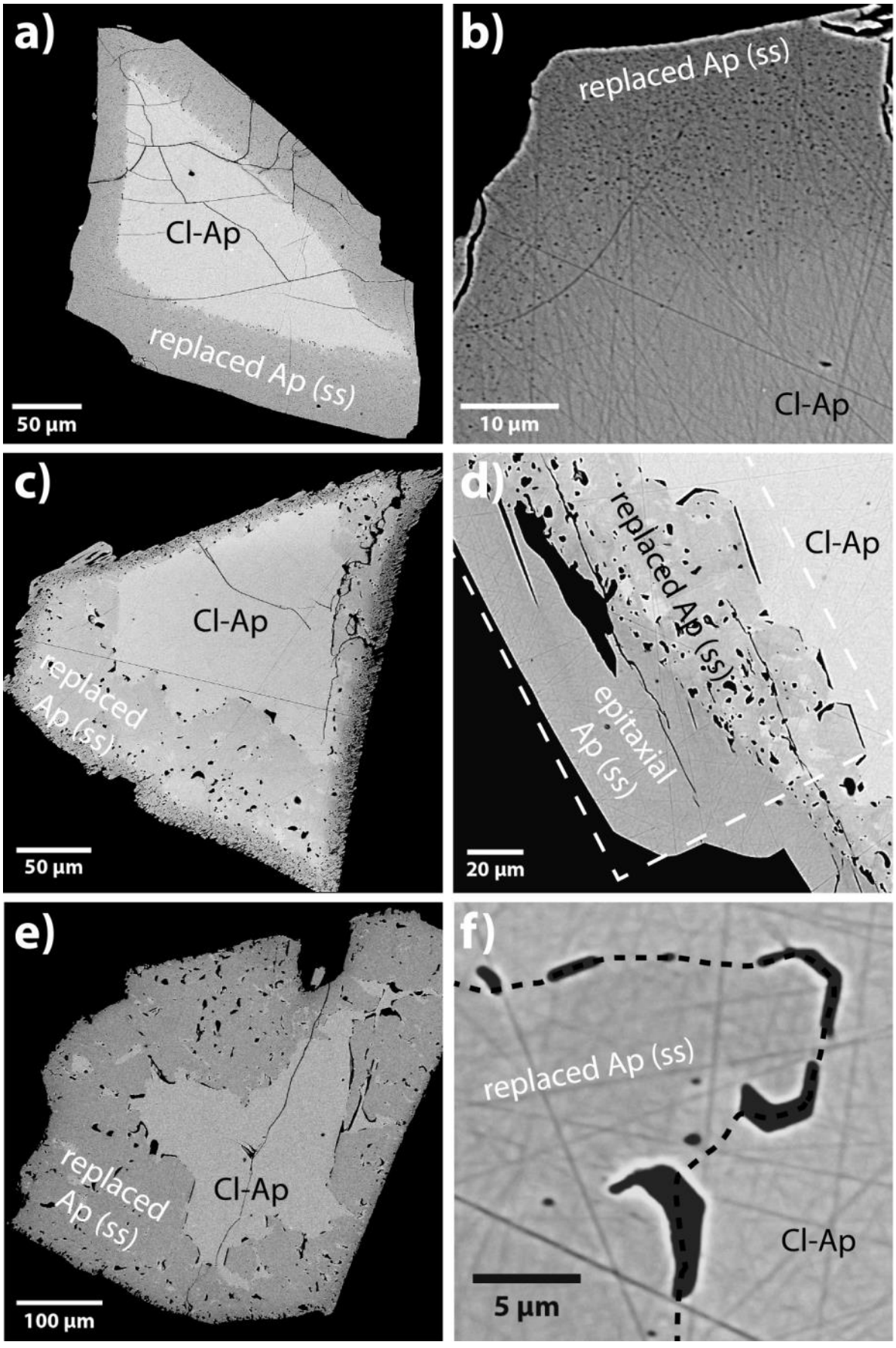
a)
Cl-Ap
replaced Ap (ss)
50 µm
b)
replaced Ap (ss)
Cl-Ap
10 µm
c)
Cl-Ap
replaced Ap (ss)
50 µm
d)
Cl-Ap
replaced Ap (ss)
epitaxial Ap (ss)
20 µm
e)
Cl-Ap
replaced Ap (ss)
100 µm
f)
replaced Ap (ss)
Cl-Ap
5 µm

1151

Figure 2

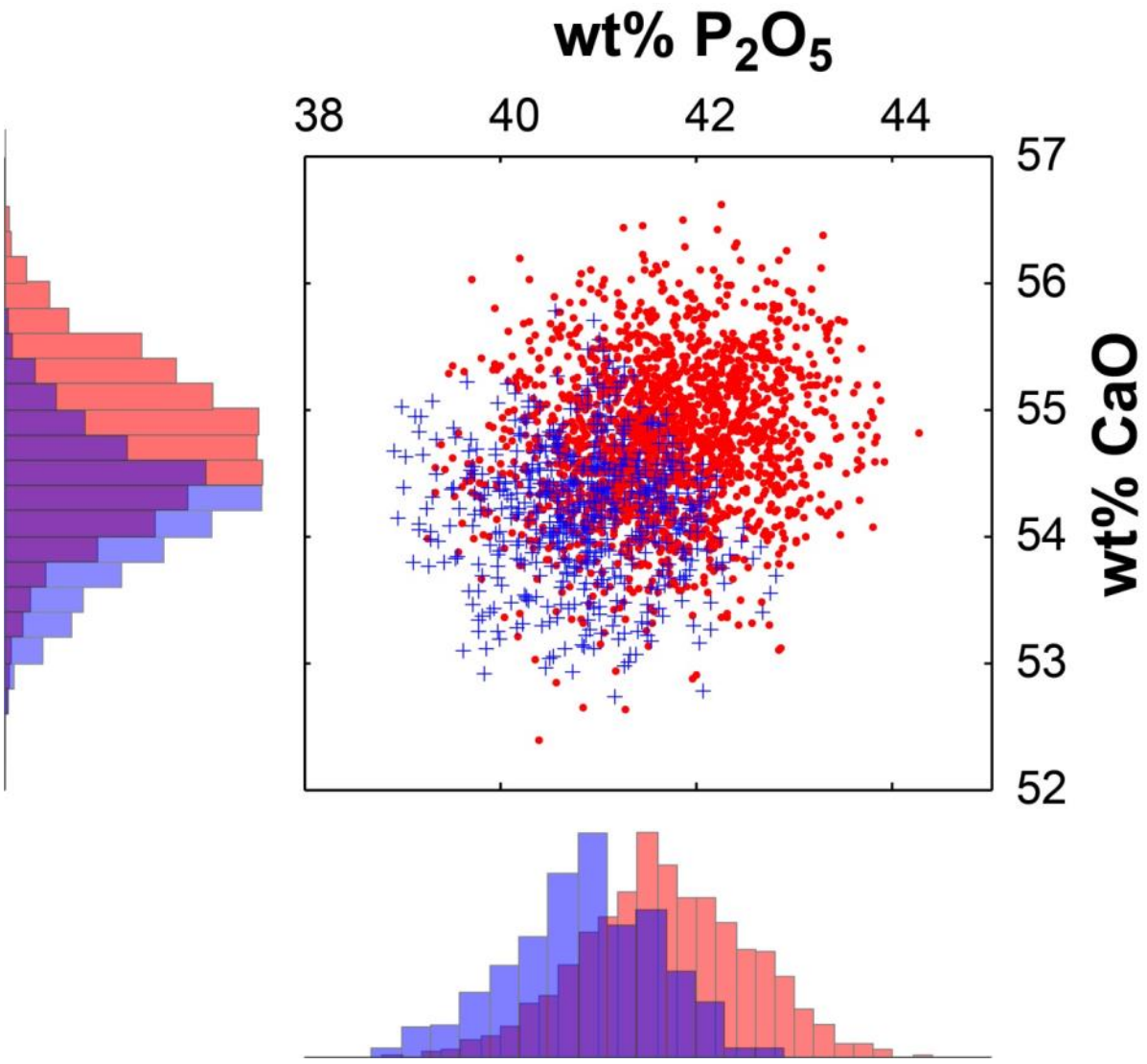

Figure 3

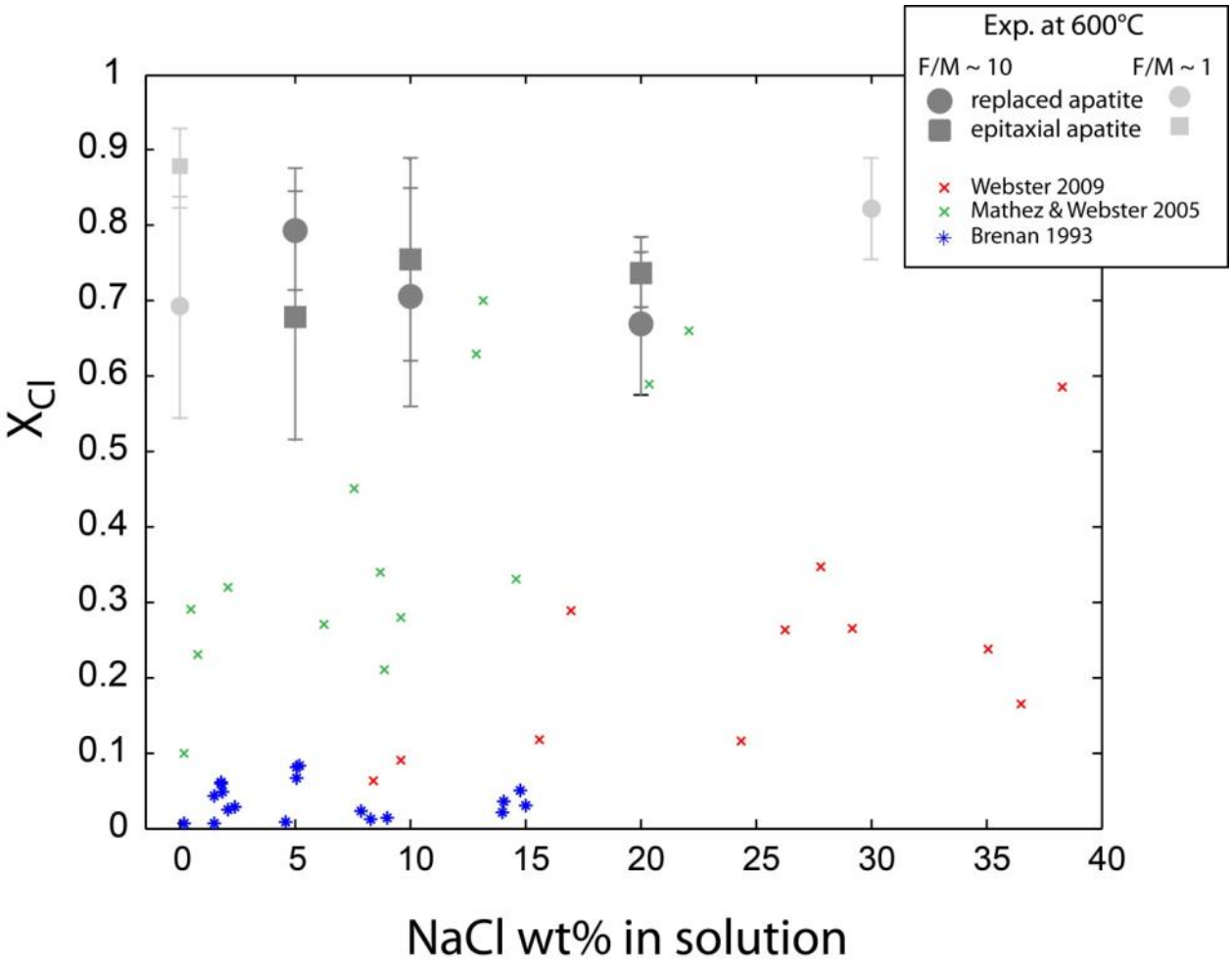

1162

1163 *Figure 4a*

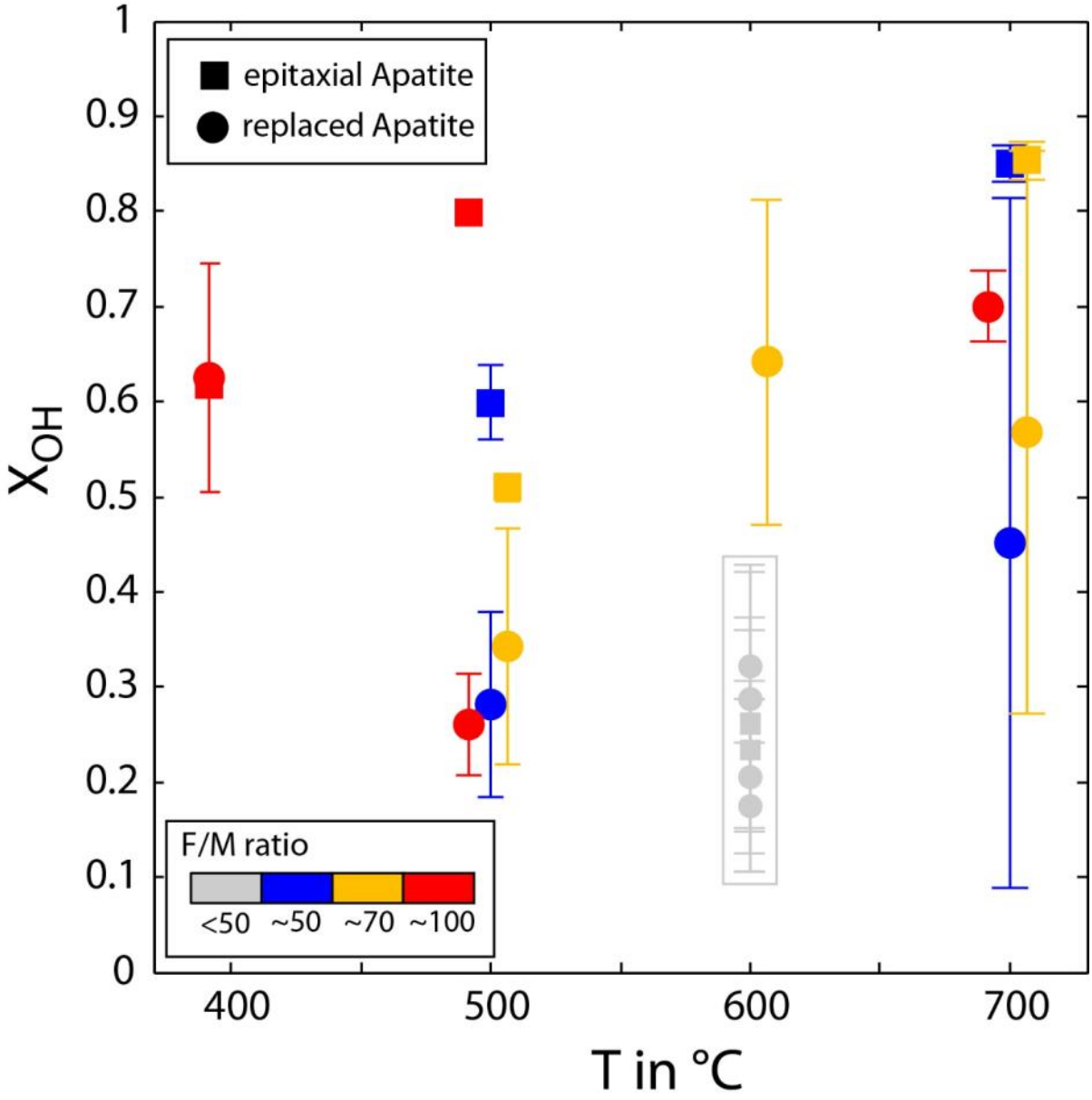
epitaxial Apatite
replaced Apatite
F/M ratio
<50 ~50 ~70 ~100
X_OH
T in °C
0
0.1
0.2
0.3
0.4
0.5
0.6
0.7
0.8
0.9
1
400
500
600
700

Figure 4b

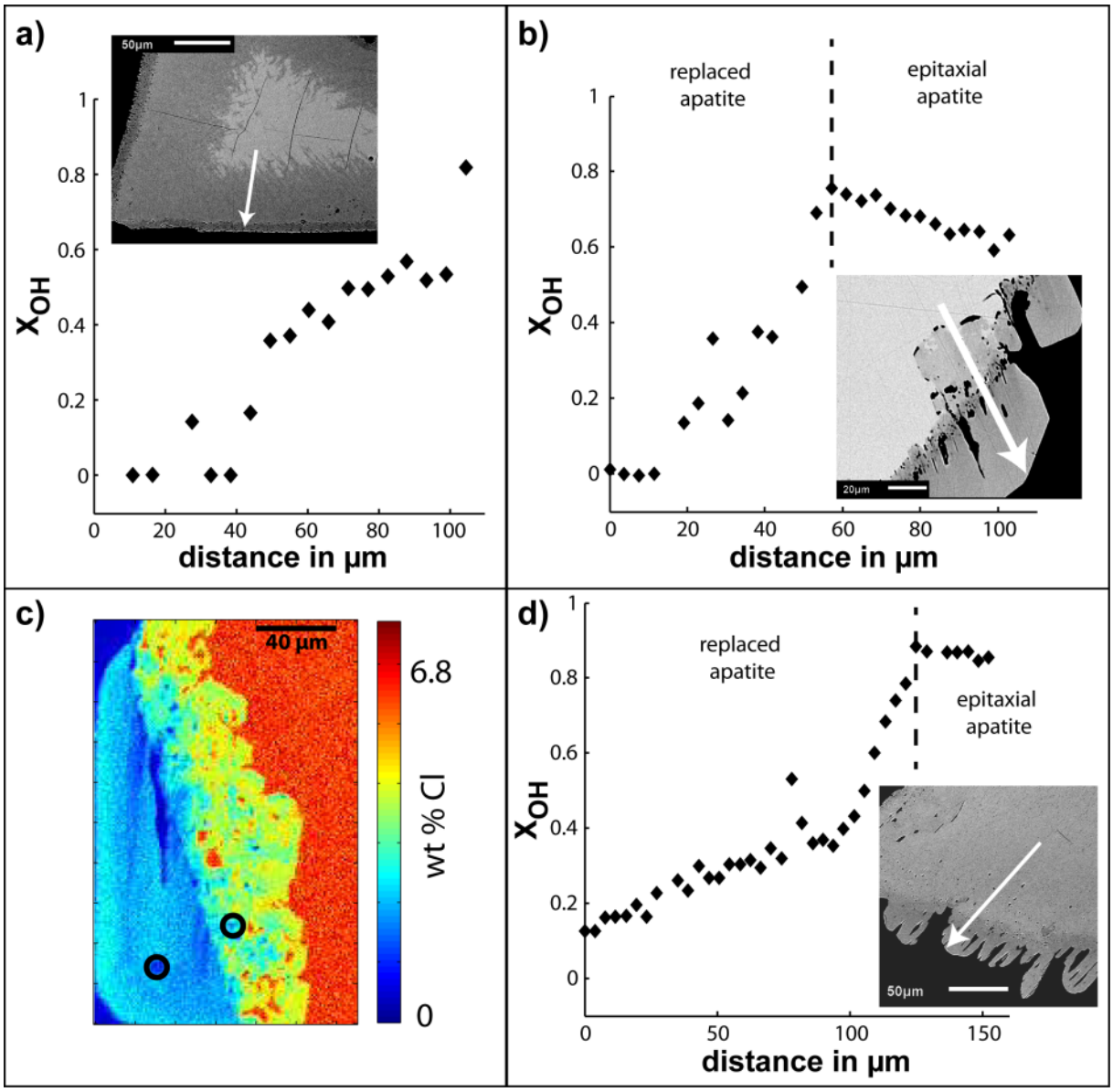
a)
50µm
1
0.8
0.6
0.4
0.2
0
X_{OH}
0
20
40
60
80
100
distance in µm
b)
replaced
apatite
epitaxial
apatite
1
0.8
0.6
0.4
0.2
0
X_{OH}
20µm
0
20
40
60
80
100
distance in µm
c)
40 µm
6.8
wt % Cl
0
d)
replaced
apatite
epitaxial
apatite
1
0.8
0.6
0.4
0.2
0
X_{OH}
50µm
0
50
100
150
distance in µm

Figure 5

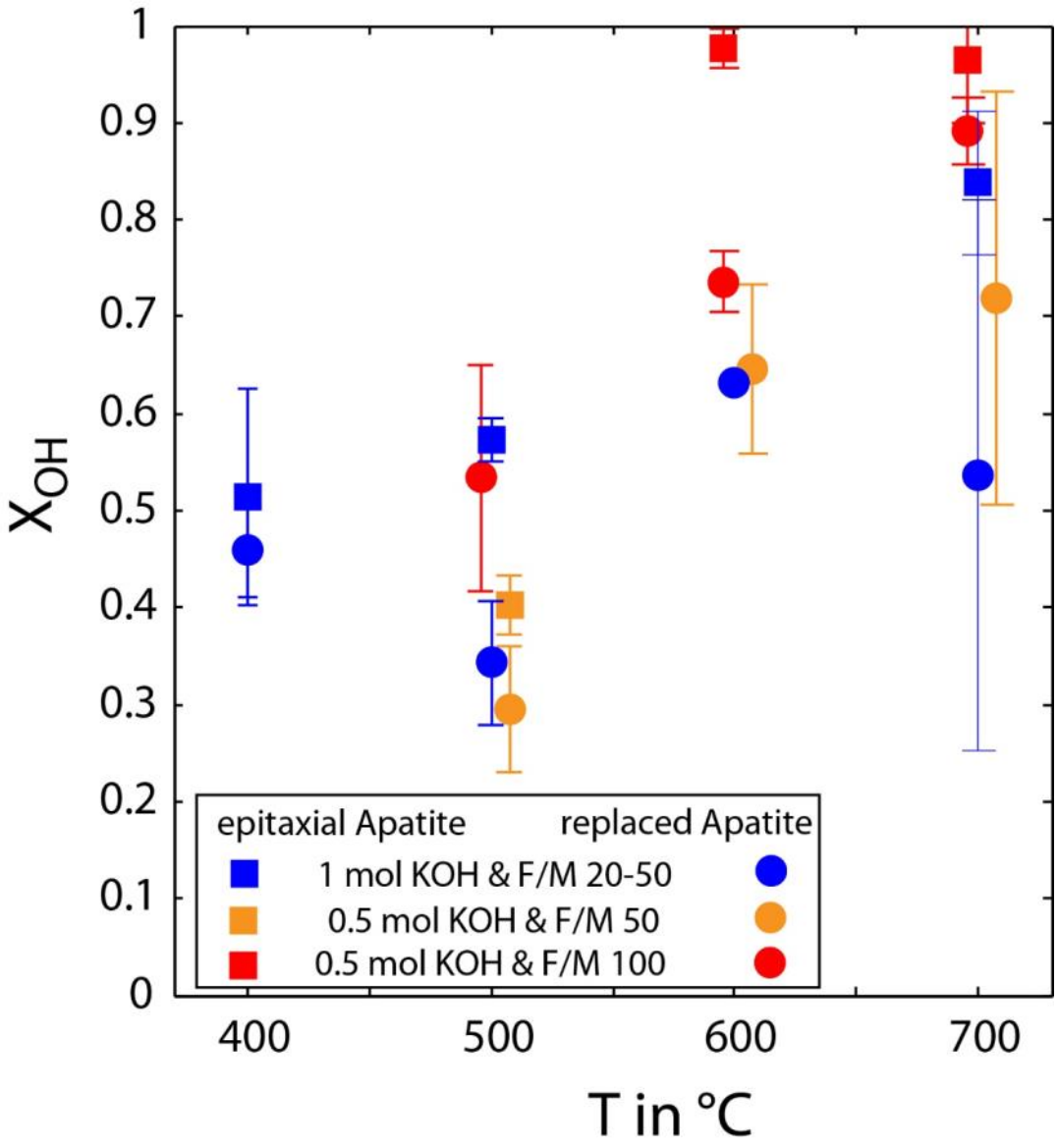
1
0.9
0.8
0.7
0.6
0.5
0.4
0.3
0.2
0.1
0
X_OH
400
500
600
700
T in °C
epitaxial Apatite
replaced Apatite
1 mol KOH & F/M 20-50
0.5 mol KOH & F/M 50
0.5 mol KOH & F/M 100

Figure 6

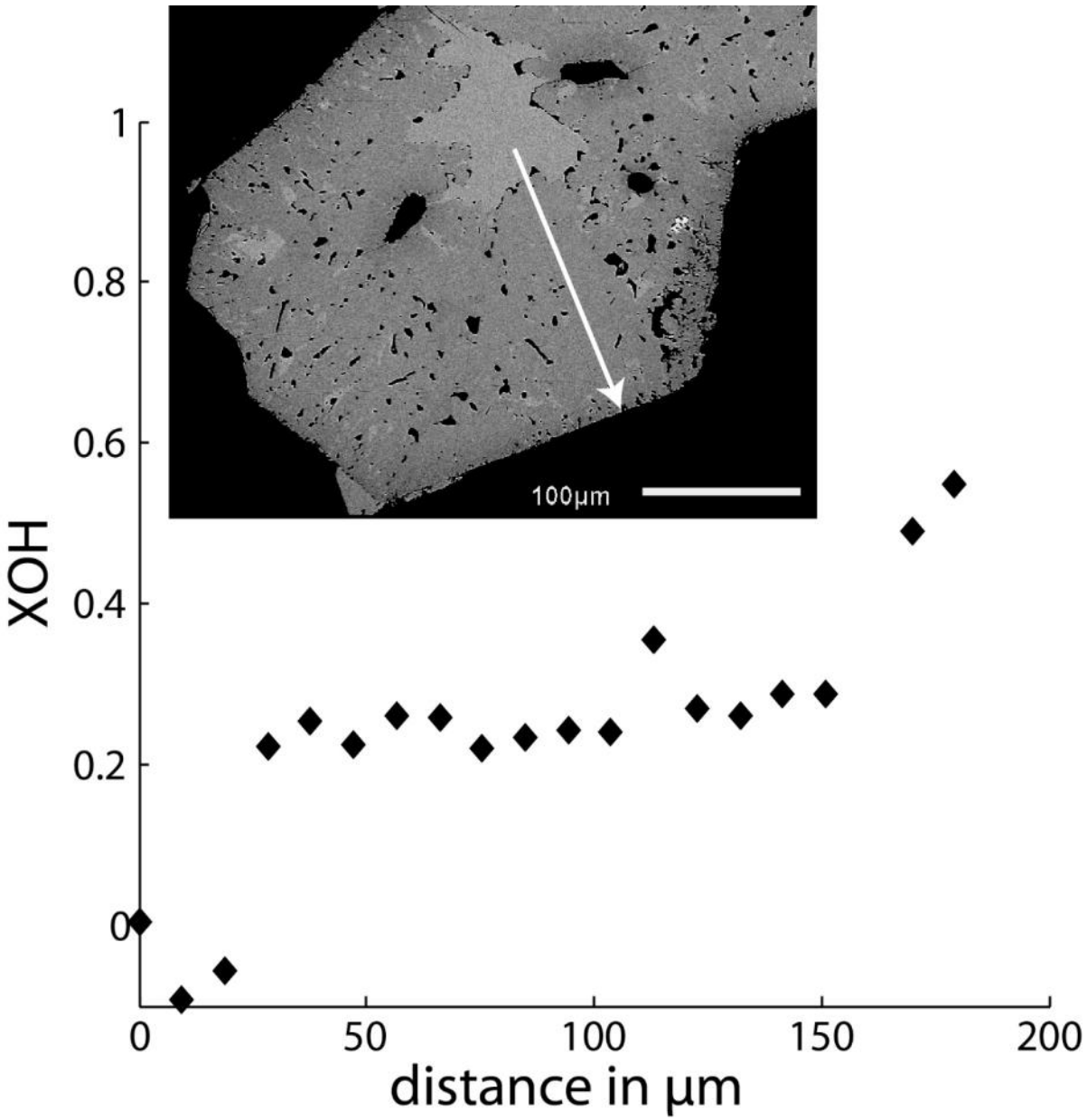

Figure 7

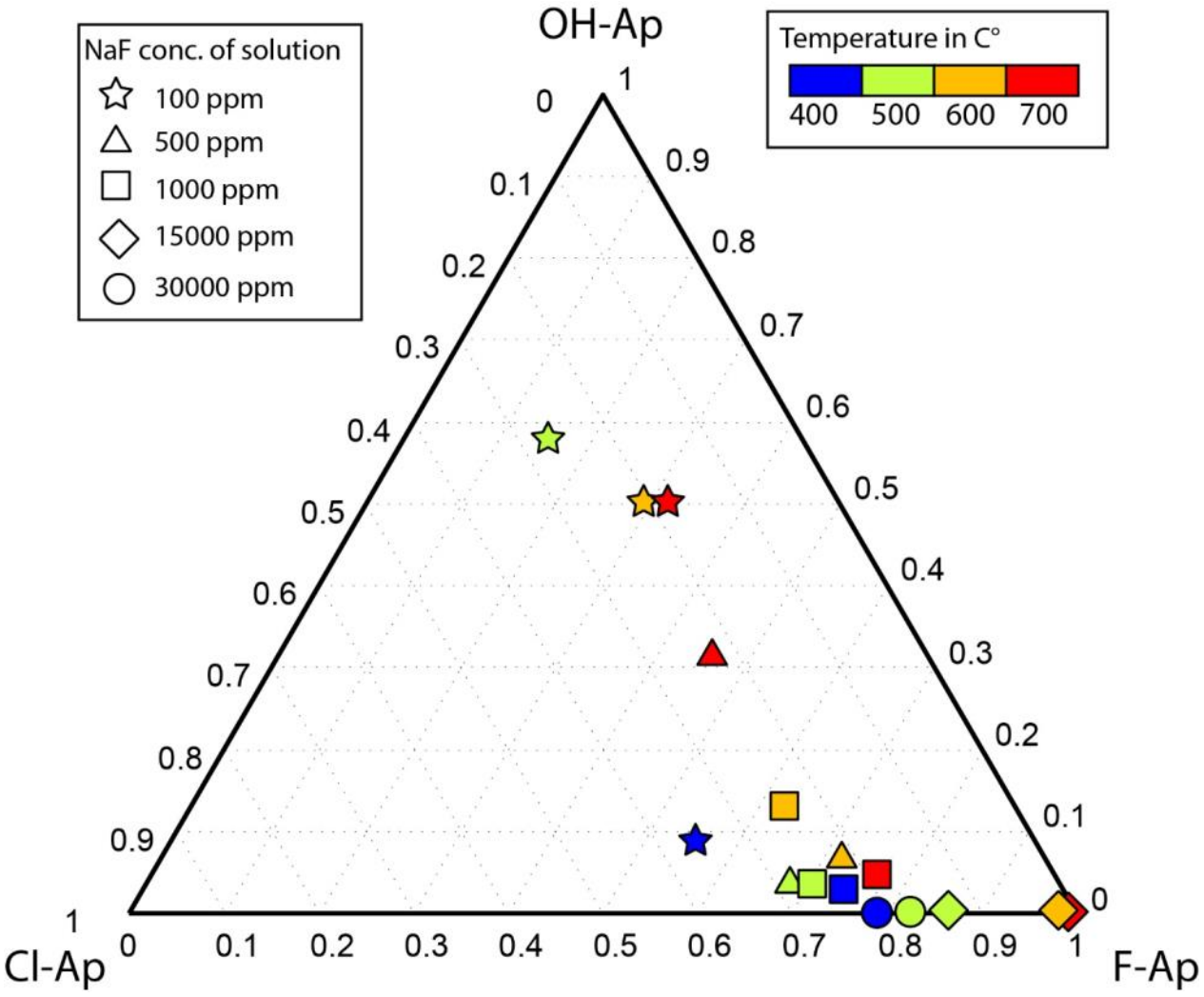
NaF conc. of solution
100 ppm
500 ppm
1000 ppm
15000 ppm
30000 ppm
OH-Ap
Temperature in C°
400
500
600
700
Cl-Ap
F-Ap
0
0.1
0.2
0.3
0.4
0.5
0.6
0.7
0.8
0.9
1

Figure 8

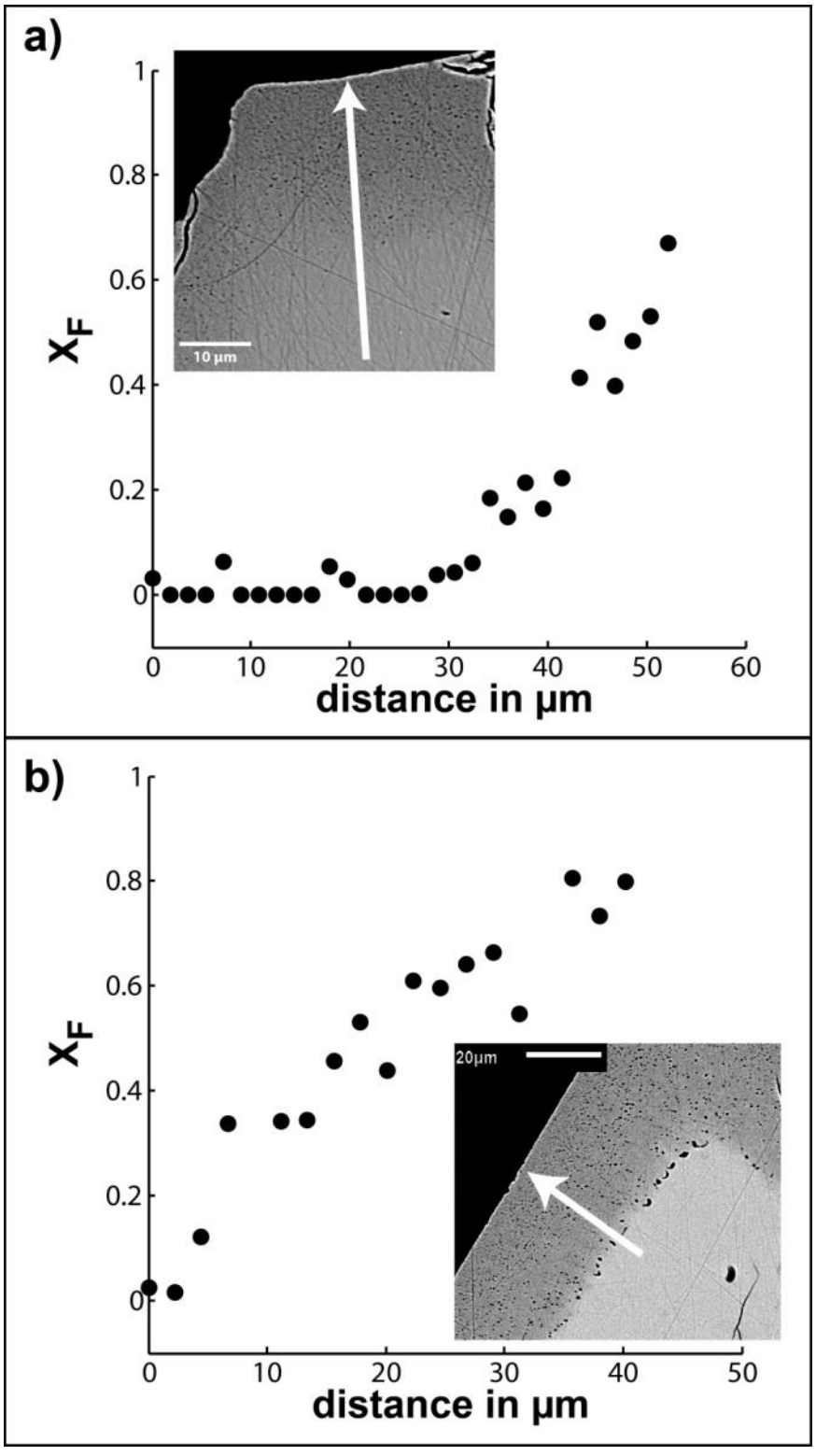
a)
1
0.8
0.6
0.4
0.2
0
x_F
10 µm
0
10
20
30
40
50
60
distance in µm
b)
1
0.8
0.6
0.4
0.2
0
x_F
20µm
0
10
20
30
40
50
distance in µm

Figure 9

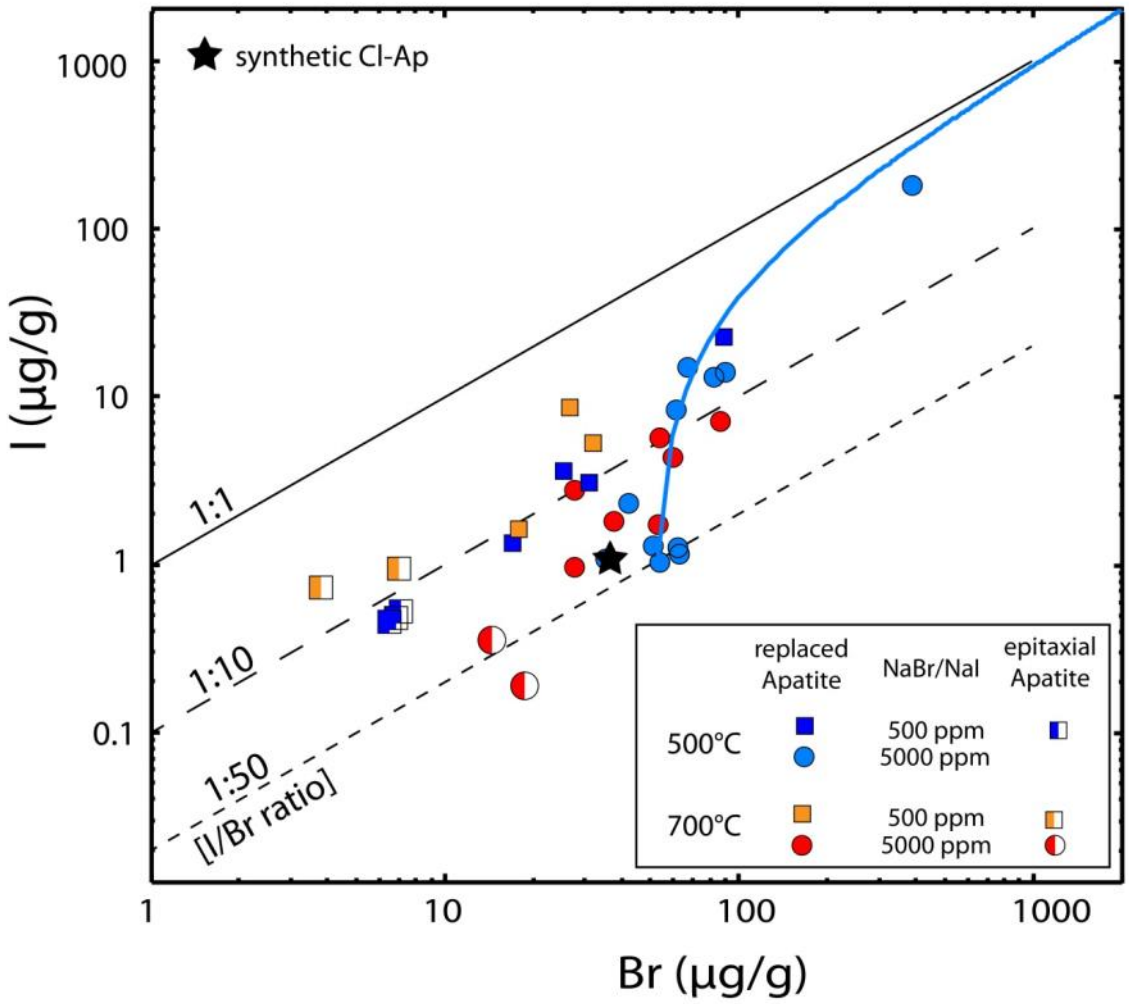

1191

1192 Figure 10a

1193

1194

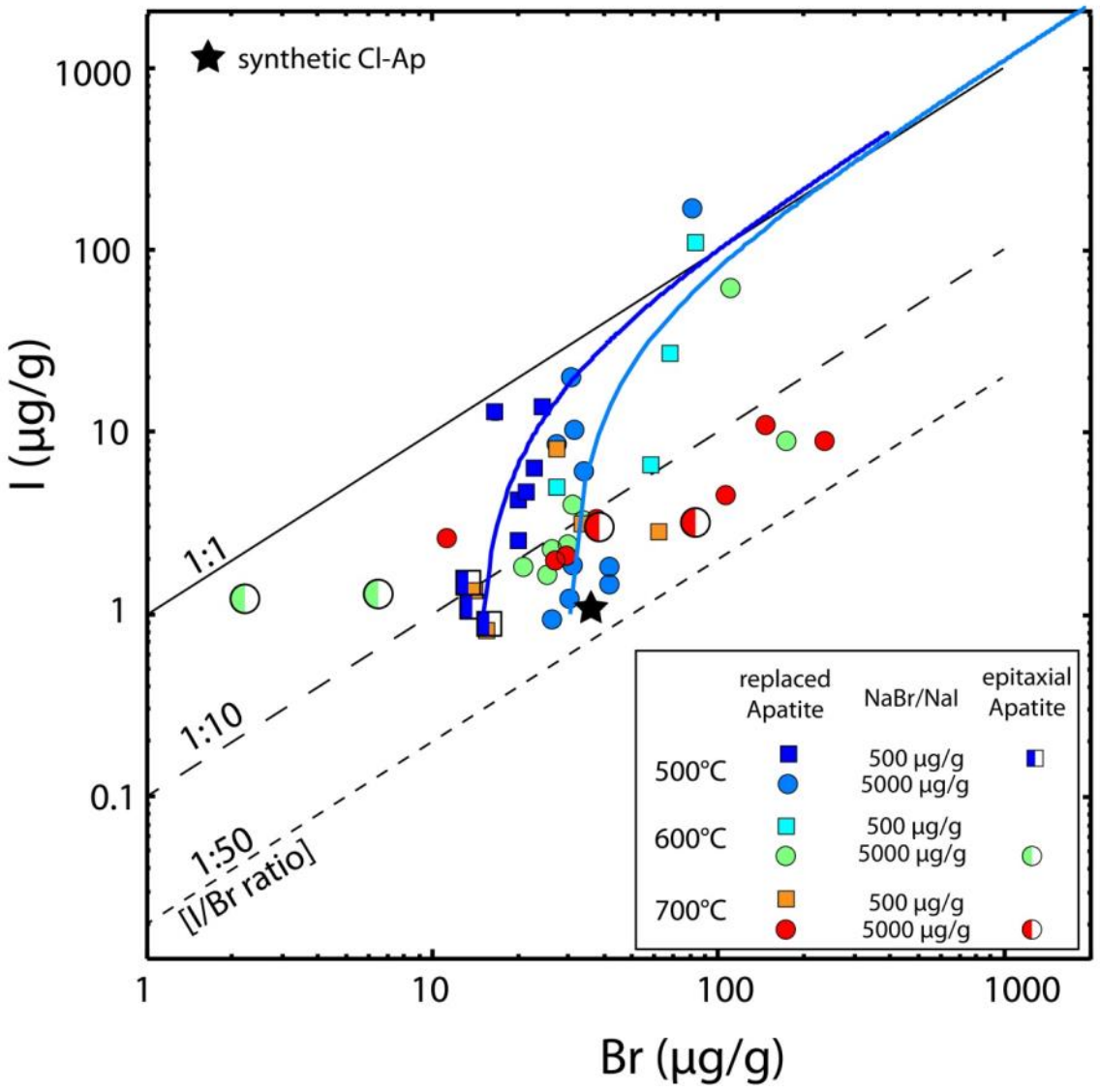
synthetic Cl-Ap
1000
100
10
1
0.1
I (µg/g)
1:1
1:10
1:50
[I/Br ratio]
1
10
100
1000
Br (µg/g)
replaced Apatite
NaBr/NaI
epitaxial Apatite
500°C
600°C
700°C
500 µg/g
5000 µg/g
500 µg/g
5000 µg/g
500 µg/g
5000 µg/g

Figure 10b

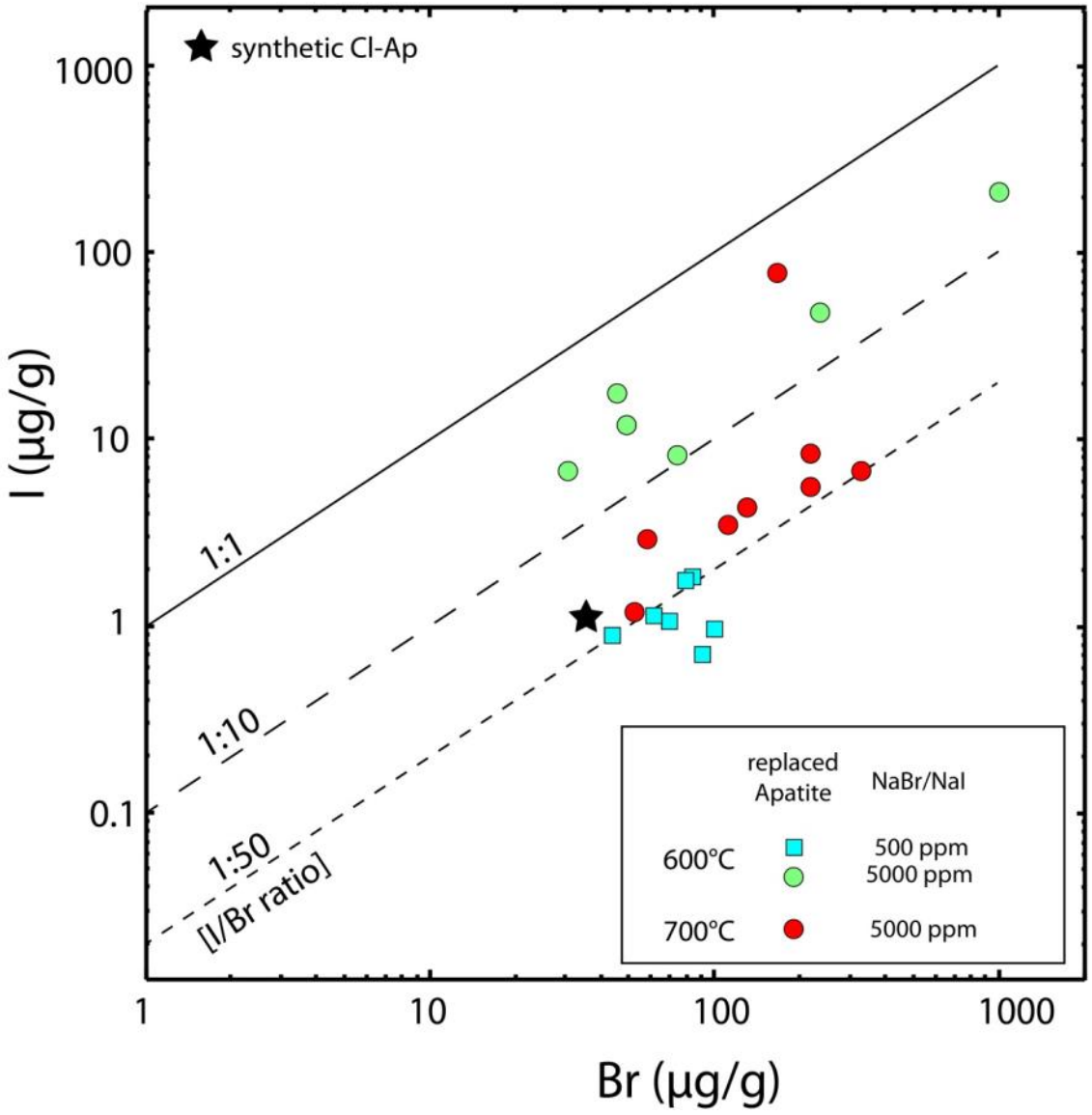

1201

1202 Figure 10c

1203

1204 -

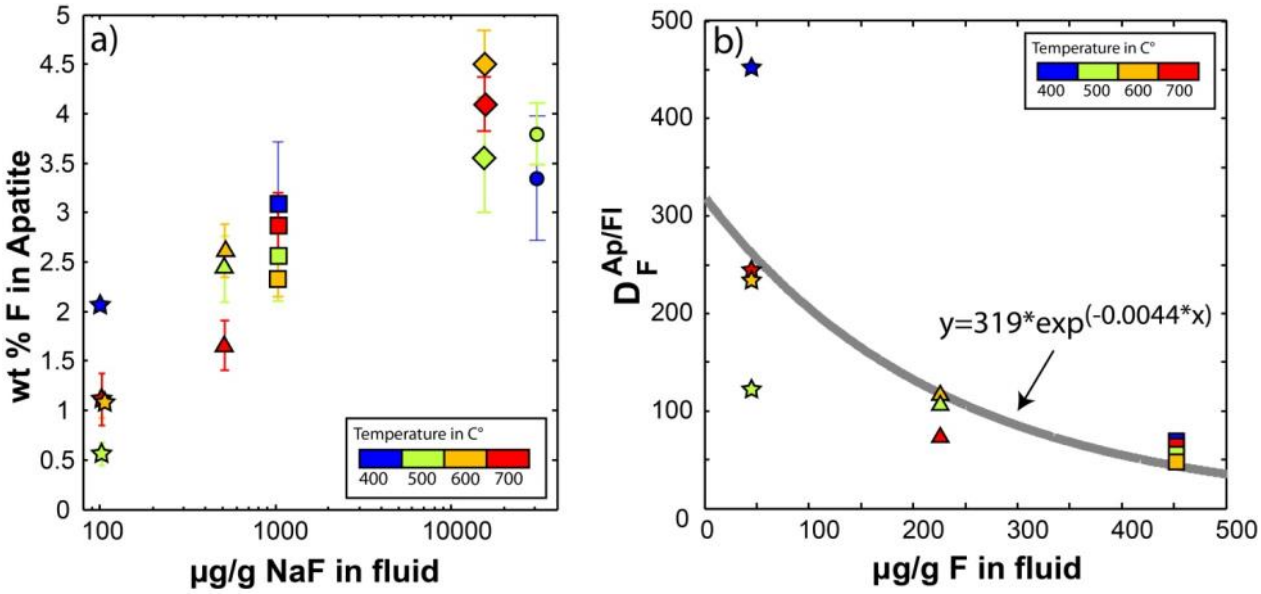

1205

1206 Figure 11

1207

1208

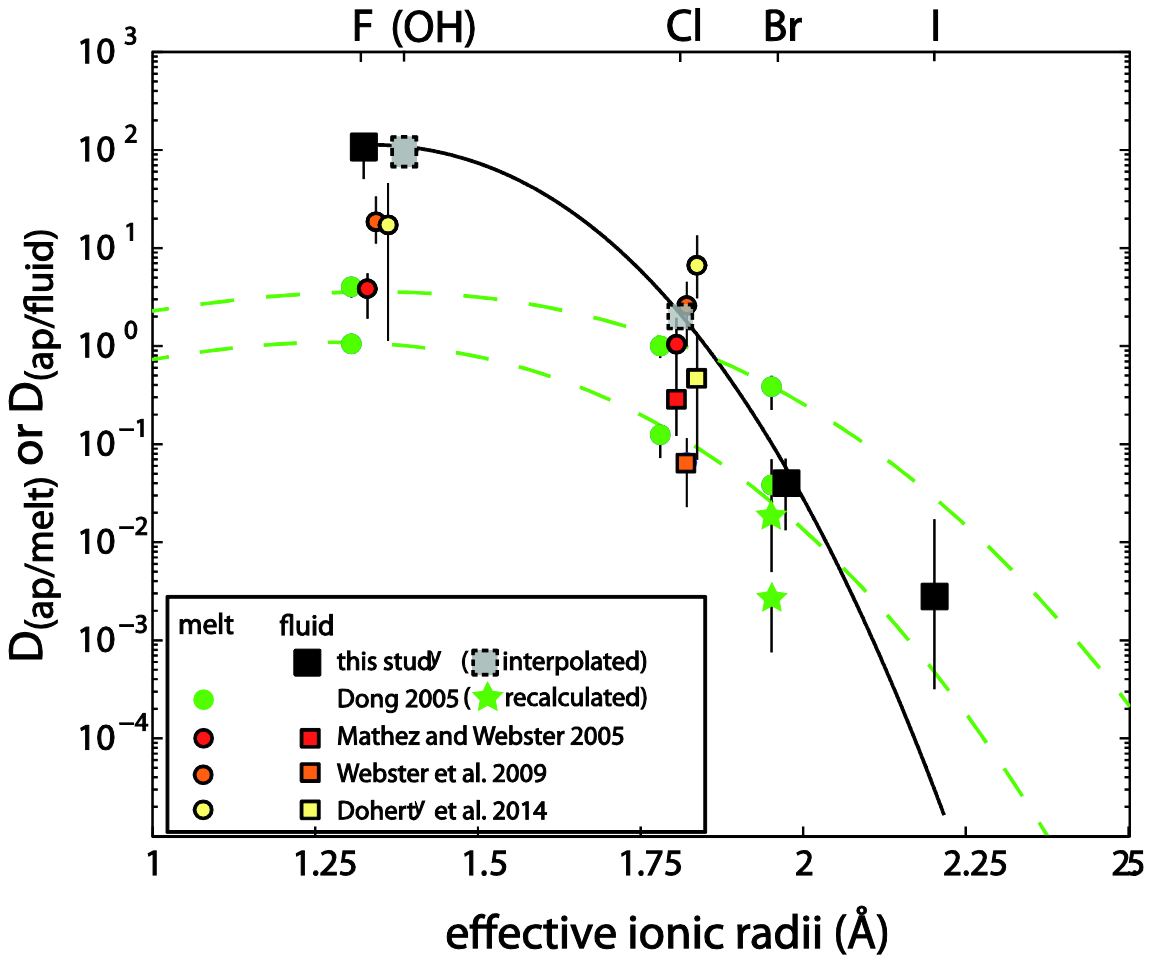

1209

1210 Fig 12

1211

1212

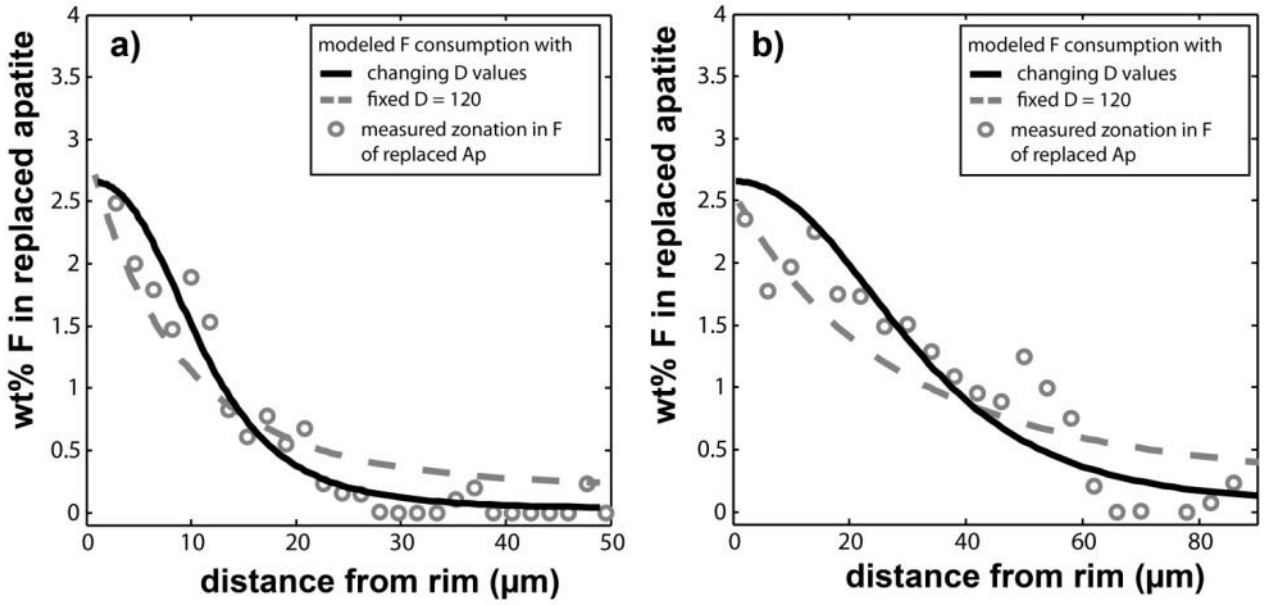

1213

1214 Figure 13

1215

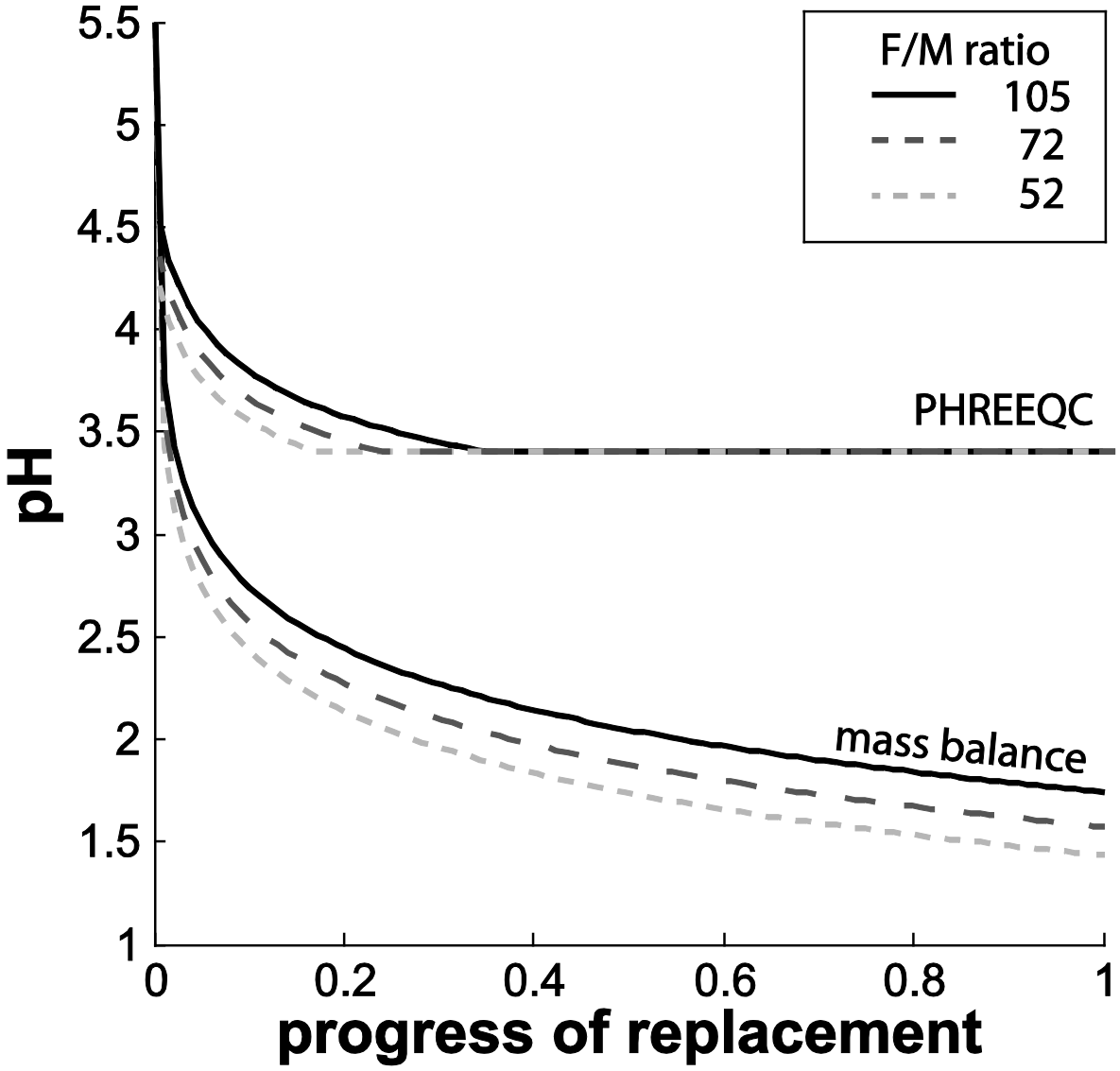
F/M ratio
105
72
52
PHREEQC
mass balance
pH
progress of replacement
5.5
5
4.5
4
3.5
3
2.5
2
1.5
1
0
0.2
0.4
0.6
0.8
1

Figure 14

1223 Tables:

1224 Table 1: Experimental conditions

Exp-Nr.	solution	Conc.	NaBr/NaI	T (°C)	F/M	t (hr)	Replace	epitaxial			replaced	
			µg/g		ratio			D_{Br}	D_I	D_F	D_{Br}	D_I
8	H_2O			700	1	1296	B					
		mol										
18	KOH	1		600	1	168	B					
20	KOH	1		600	27	168	A+B					
22	KOH	1		600	10	168	B					
32	KOH	1		400	22	168	B					
34	KOH	1		700	51	168	B					
41	KOH	1		500		168	B					
59	KOH	0.5	500	500	45	336	B	0.037	0.0030		0.054	0.0175
62	KOH	0.5	500	700	52	336	A				0.038	0.0025
69	KOH	0.5	500	600	48	336	B				0.152	0.0135
73	KOH	0.5	5000	700	103	408	A+B	0.016	0.0007		0.007	0.0006
86	KOH	0.5	5000	500	120	408	A				0.009	0.0003
87	KOH	0.5	5000	600	128	408	A	0.001	0.0003		0.007	0.0006
		wt%										
9	NaCl	30%		600	1	72	B					
29	NaCl	5%		600	10	168	B					
30	NaCl	10%		600	11	168	A+B					
31	NaCl	20%		600	11	168	B					
35	NaCl	10%		400	105	168	B					
36	NaCl	10%		500	72	168	B					
42	NaCl	10%		700		168	A					
63	NaCl	5%	500	500	52	336	B	0.018	0.0012		0.064	0.0063
65	NaCl	5%	500	700	51	336	A	0.014	0.0020		0.066	0.0119
74	NaCl	10%	5000	500	105	408	B				0.013	0.0003
76	NaCl	10%	5000	700	69	408	A	0.004	0.0001		0.013	0.0008
88	NaCl	10%	5000	600	67	408	A					
		µg/g										
47	NaF	100		700	100	168	A			245		
48	NaF	1000		700	99	168	A			63		
50	NaF	100		500	60	168	A			123		
51	NaF	1000		500	74	168	A			57		
52	NaF	30000		500	85	168	A+B					
53	NaF	100		400	101	168	A			453		
54	NaF	1000		400	100	168	A			68		
55	NaF	30000		400	90	168	A					
56	NaF	1000		600	98	168	A			52		
57	NaF	100		600	47	168	A			234		
58	NaF	500	500	700	34	336	A			73		
66	NaF	500	500	500	37	336	A			107		
67	NaF	500	500	600	50	336	A			115	0.192	0.0028
89	NaF	15000	5000	500	101	408	A					
90	NaF	15000	5000	600	99	408	A				0.013	0.0026
91	NaF	15000	5000	700	75	408	A				0.041	0.0011

1225

1226 Table 2: EMPA major element data for replaced and epitaxial apatite

Exp-Nr.	replaced Apatite CaO	P_2O_5	Cl	F	OH	X_{Cl}	X_F	X_{OH}
8	55.30 ± 0.70	41.08 ± 1.59	4.70 ± 0.94		0.54 ± 0.26	0.69 ± 0.15		0.31 ± 0.15
18	54.41 ± 0.16	40.58 ± 1.10	5.49 ± 0.65		0.32 ± 0.19	0.81 ± 0.11		0.19 ± 0.11
20	54.88 ± 0.00	41.47 ± 0.00	2.49 ± 0.00		1.08 ± 0.00	0.37 ± 0.00		0.63 ± 0.00
22	55.30 ± 0.10	41.37 ± 1.51	4.40 ± 0.16		0.62 ± 0.08	0.64 ± 0.04		0.36 ± 0.04
32	54.85 ± 0.49	42.08 ± 0.85	3.66 ± 0.32		0.80 ± 0.09	0.53 ± 0.05		0.46 ± 0.05
34	54.43 ± 0.37	41.67 ± 0.80	3.13 ± 1.94		0.92 ± 0.49	0.46 ± 0.28		0.54 ± 0.28
41	54.79 ± 0.42	41.56 ± 0.83	4.38 ± 0.35		0.60 ± 0.11	0.64 ± 0.05		0.34 ± 0.06
59	54.41 ± 0.71	41.61 ± 0.76	4.80 ± 0.42		0.51 ± 0.11	0.70 ± 0.07		0.30 ± 0.07
62	55.12 ± 0.35	42.42 ± 0.46	1.78 ± 1.54		1.25 ± 0.37	0.26 ± 0.22		0.72 ± 0.21
69	54.79 ± 0.37	41.95 ± 0.66	2.22 ± 0.72		1.11 ± 0.15	0.33 ± 0.10		0.65 ± 0.09
73	54.13 ± 0.77	42.15 ± 0.42	0.73 ± 0.25		1.52 ± 0.05	0.11 ± 0.04		0.89 ± 0.03
86	54.78 ± 0.50	42.17 ± 0.95	3.11 ± 0.85		0.93 ± 0.20	0.45 ± 0.12		0.53 ± 0.12
87	54.37 ± 0.41	41.55 ± 0.33	1.69 ± 0.21		1.26 ± 0.05	0.25 ± 0.03		0.74 ± 0.03
9	54.55 ± 0.58	41.09 ± 0.65	5.61 ± 0.47		0.30 ± 0.12	0.82 ± 0.07		0.17 ± 0.07
29	54.61 ± 0.37	40.84 ± 0.39	5.39 ± 0.57		0.35 ± 0.14	0.79 ± 0.08		0.21 ± 0.08
30	54.50 ± 0.55	41.39 ± 0.73	4.81 ± 1.00		0.50 ± 0.24	0.71 ± 0.14		0.29 ± 0.14
31	54.74 ± 0.33	42.01 ± 0.88	4.60 ± 0.62		0.56 ± 0.18	0.67 ± 0.09		0.32 ± 0.10
35	54.81 ± 0.56	42.14 ± 0.74	2.49 ± 0.86		1.08 ± 0.21	0.37 ± 0.13		0.62 ± 0.12
36	54.75 ± 0.33	41.25 ± 0.74	4.41 ± 0.82		0.59 ± 0.21	0.65 ± 0.12		0.34 ± 0.12
42	54.82 ± 0.51	42.25 ± 0.77	1.99 ± 0.23		1.21 ± 0.07	0.29 ± 0.03		0.70 ± 0.04
63	54.30 ± 0.45	41.71 ± 0.74	4.87 ± 0.64		0.49 ± 0.17	0.71 ± 0.10		0.28 ± 0.10
65	54.68 ± 0.44	41.56 ± 1.18	3.70 ± 2.50		0.78 ± 0.63	0.54 ± 0.37		0.45 ± 0.36
74	54.50 ± 0.37	41.42 ± 0.84	5.04 ± 0.35		0.45 ± 0.09	0.74 ± 0.05		0.26 ± 0.05
76	54.87 ± 0.53	41.80 ± 0.67	2.90 ± 2.03		0.98 ± 0.51	0.43 ± 0.30		0.57 ± 0.30
88	54.91 ± 0.54	42.08 ± 1.02	2.40 ± 1.12		1.11 ± 0.28	0.35 ± 0.16		0.64 ± 0.17
47	54.93 ± 0.80	42.09 ± 0.17	1.43 ± 0.58	1.11 ± 0.26	0.85 ± 0.04	0.21 ± 0.08	0.30 ± 0.07	0.49 ± 0.02
48	55.02 ± 0.63	42.16 ± 0.75	1.32 ± 0.29	2.87 ± 0.33	0.08 ± 0.10	0.19 ± 0.04	0.76 ± 0.09	0.05 ± 0.06
50	54.81 ± 0.30	42.08 ± 0.70	1.86 ± 0.23	0.56 ± 0.12	1.00 ± 0.07	0.27 ± 0.03	0.15 ± 0.03	0.58 ± 0.04
51	55.28 ± 0.90	41.68 ± 0.56	1.76 ± 0.35	2.56 ± 0.46	0.10 ± 0.19	0.25 ± 0.05	0.69 ± 0.12	0.06 ± 0.11
52	54.62 ± 0.42	41.91 ± 0.71	0.80 ± 0.37	3.79 ± 0.31	-0.22 ± 0.15	0.11 ± 0.05	1.01 ± 0.09	-0.12 ± 0.09
53	55.81 ± 0.43	41.75 ± 0.73	2.29 ± 0.51	2.05 ± 0.03	0.22 ± 0.13	0.33 ± 0.07	0.55 ± 0.00	0.12 ± 0.07
54	55.45 ± 0.19	42.72 ± 0.51	1.69 ± 0.59	3.10 ± 0.62	-0.10 ± 0.19	0.24 ± 0.08	0.82 ± 0.16	-0.05 ± 0.11

55	55.49	±	0.61	42.04	±	0.45	1.55	±	1.03	3.35	±	0.63	-0.19	±	0.10	0.22	±	0.15	0.89	±	0.17	-0.11	±	0.05
56	55.00	±	0.48	42.20	±	0.75	1.70	±	0.29	2.34	±	0.19	0.23	±	0.09	0.24	±	0.04	0.63	±	0.05	0.13	±	0.05
57	55.22	±	0.55	42.07	±	0.79	1.70	±	0.79	1.06	±	0.14	0.81	±	0.16	0.25	±	0.12	0.29	±	0.03	0.46	±	0.09
58	55.18	±	0.66	42.15	±	0.78	1.54	±	0.38	1.66	±	0.25	0.58	±	0.11	0.22	±	0.06	0.45	±	0.07	0.33	±	0.06
66	54.88	±	0.44	41.29	±	0.58	2.02	±	0.33	2.43	±	0.33	0.09	±	0.11	0.29	±	0.05	0.66	±	0.09	0.05	±	0.06
67	55.01	±	0.24	41.75	±	1.03	1.50	±	0.16	2.62	±	0.27	0.14	±	0.12	0.22	±	0.02	0.70	±	0.07	0.08	±	0.07
89	54.49	±	0.88	40.93	±	0.31	1.76	±	0.99	3.55	±	0.55	-0.37	±	0.08	0.25	±	0.14	0.95	±	0.14	-0.21	±	0.05
90	55.37	±	0.79	41.75	±	0.16	0.10	±	0.09	4.50	±	0.34	-0.37	±	0.19	0.01	±	0.01	1.19	±	0.09	-0.21	±	0.11
91	55.44	±	0.63	42.29	±	0.76	0.08	±	0.06	4.10	±	0.27	-0.17	±	0.13	0.01	±	0.01	1.08	±	0.07	-0.09	±	0.07

1227

Exp-Nr.	epitaxial Apatite CaO			P_2O_5			Cl			F	OH			X_{Cl}			X_F	X_{OH}		
8	54.63	±	0.52	41.01	±	0.66	5.99	±	0.37		0.20	±	0.09	0.88	±	0.05		0.11	±	0.05
18																				
20																				
22																				
32	54.92	±	0.62	41.98	±	0.65	3.24	±	0.76		0.89	±	0.19	0.47	±	0.11		0.51	±	0.11
34	54.76	±	0.75	42.27	±	0.75	1.01	±	0.53		1.44	±	0.13	0.15	±	0.08		0.84	±	0.07
41	54.91	±	0.57	42.19	±	0.92	2.88	±	0.12		1.00	±	0.05	0.42	±	0.02		0.57	±	0.02
59	54.67	±	0.41	41.86	±	0.38	3.93	±	0.20		0.70	±	0.05	0.57	±	0.03		0.40	±	0.03
62																				
69																				
73	55.36	±	0.23	42.46	±	0.51	0.05	±	0.02		1.66	±	0.10	0.01	±	0.00		0.96	±	0.07
86																				
87	55.60	±	0.37	42.43	±	0.77	0.09	±	0.07		1.69	±	0.04	0.01	±	0.01		0.98	±	0.02
9																				
29	54.61	±	0.53	40.95	±	0.80	4.60	±	1.06		0.45	±	0.20	0.68	±	0.16		0.26	±	0.11
30	54.43	±	0.96	40.91	±	1.15	5.10	±	0.86		0.40	±	0.23	0.75	±	0.13		0.23	±	0.13
31	54.66	±	0.35	42.09	±	0.78	5.09	±	0.29		0.46	±	0.08	0.74	±	0.05		0.26	±	0.05
35	55.25	±	0.00	41.68	±	0.00	2.56	±	0.00		1.06	±	0.00	0.38	±	0.00		0.62	±	0.00
36	54.89	±	0.63	41.43	±	0.93	3.16	±	0.07		0.88	±	0.01	0.47	±	0.02		0.51	±	0.01
42																				
63	54.82	±	0.59	41.47	±	0.66	2.61	±	0.17		1.03	±	0.06	0.39	±	0.02		0.60	±	0.04
65	55.46	±	0.19	41.68	±	1.29	0.94	±	0.04		1.46	±	0.01	0.14	±	0.00		0.85	±	0.02
74	54.57	±	0.61	42.11	±	0.55	1.37	±	0.05		1.37	±	0.02	0.20	±	0.01		0.80	±	0.01
76	55.23	±	0.67	42.23	±	0.66	0.95	±	0.05		1.47	±	0.04	0.14	±	0.01		0.85	±	0.02